Electronic Supplementary Material (ESI) for Journal of Materials Chemistry C.

Supporting Information

Structure-function relationship exploration for enhanced thermal stability and electro-optic activity in monolithic organic NLO chromophores

Wenwei Jin,[ab] Peter V. Johnston,[b] Delwin L. Elder,*[b] Karl T. Manner,[b] Kerry E. Garrett,[b] Werner Kaminsky,[b] Ruimin Xu,[a] Bruce H. Robinson[b] and Larry R. Dalton[b]

[a]EHF Key Laboratory of Fundamental Science, University of Electronic Science and Technology of China, Chengdu 611731, P. R. China

[b]Department of Chemistry, Box 351700, University of Washington, Seattle, Washington 98195, United States

Experimental Section:

General information: Chemicals used were purchased from Sigma Aldrich, Acros, Alfa Aesar, or TCI and used without further purification unless otherwise noted. 1,1,2 trichloroethane (TCE) was purified via vacuum distillation prior to use. ITO/glass slides were purchased from Thin Film Devices, Inc. Optical profilometry measurements were carried out on an NT-2000 model profilometer, provided by WYKO Corporation. *In situ* Teng-Man ellipsometry was carried out on a home built device.[1] UV-visible Absorption Spectroscopy was obtained on a Shimadzu 1601 or a Varian Cary 5000 spectrometer. Differential Scanning Calorimetry (DSC) data was acquired on a TA Instruments Q100 with heating and cooling under nitrogen at rates of 10 °C per min. Thermogravametric Analysis (TGA) data was acquired on a TA Instruments Q500 with heating under nitrogen at 20 °C per min. TGA and DSC analyses were carried out at the Advanced Materials Science and Engineering Center (AMSEC) at Western Washington University. High-Resolution Mass Spectrometry (HRMS) was performed using a Waters Micromass Quattro Premier XW instrument using electrospray ionization to acquire a high resolution spectrum. ^{1}H NMR spectra were acquired using a Bruker AVance ugseries instrument running at 300 MHz or 500 MHz. All ^{13}C NMR spectra were acquired on a Bruker AVance 500 MHz instrument.

Synthetic details: The synthesis of organic ring-locked tetraene donor−π−acceptor molecules was accomplished via the trinary convergent synthesis of the donor, the bridge, and the acceptor.

Once these three components are synthesized, they can be assembled in any order.[2] Several authors have previously published syntheses outlining various substitutions and methods to synthesize various analogues of this class of molecules.[3-7] Here we present a detailed method for the synthesis of YLD-124 with recent modifications and additional details for the synthesis of analogues. In some cases, where the molecules were not new or reaction methods were the same, characterization of intermediates was limited to TLC.

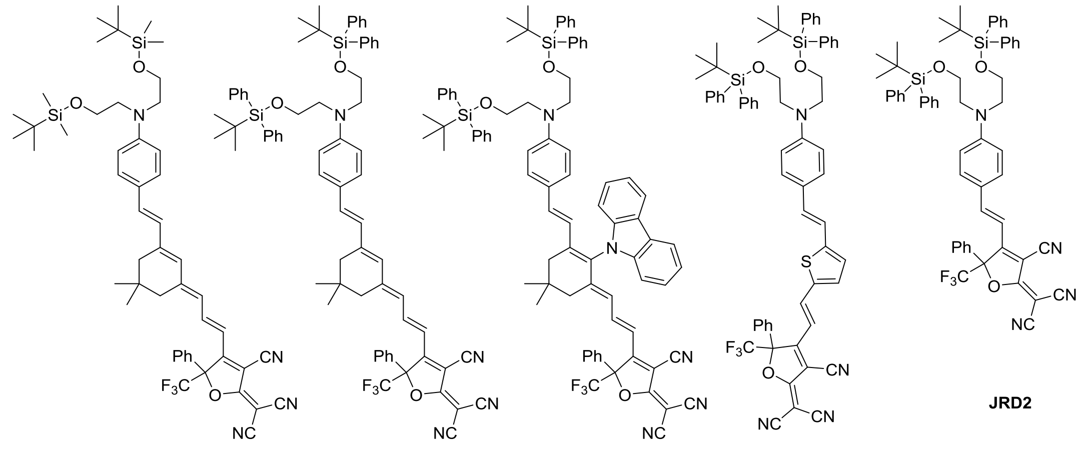

YLD-124 **JRD1** **JRD5** **KRD1** **JRD2**

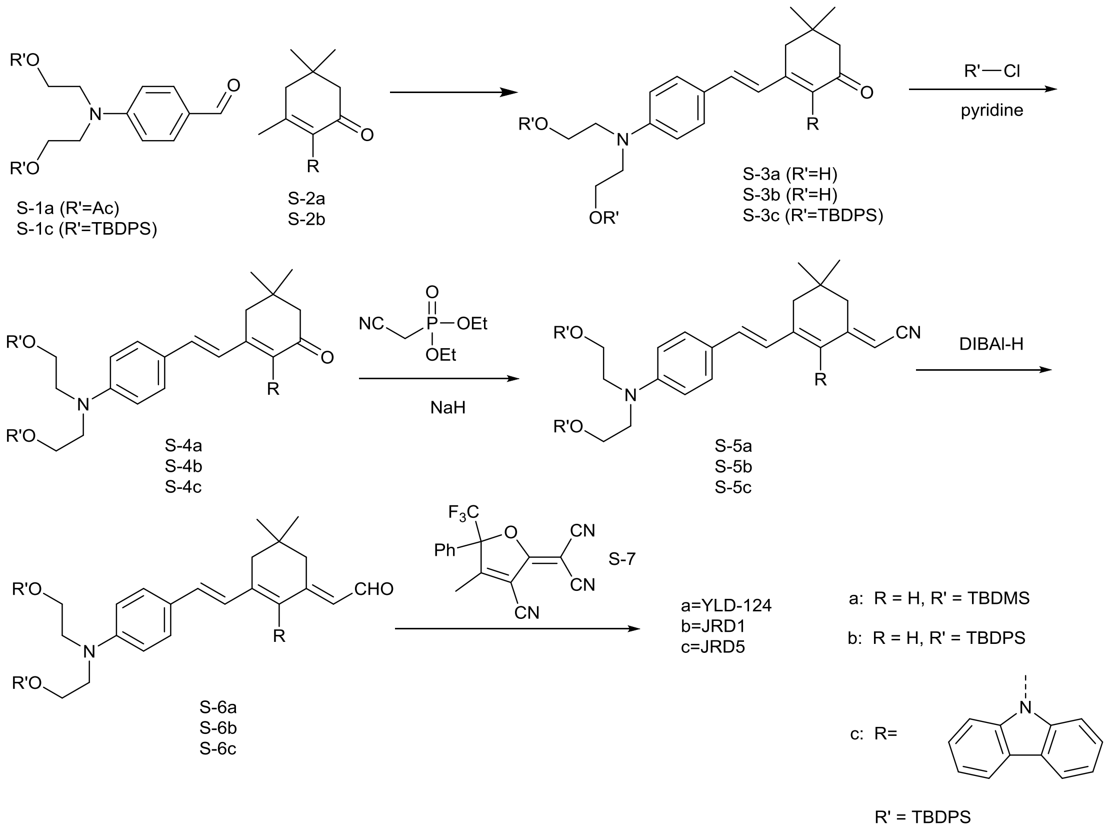

YLD-124:

3-[2-[4-[bis(2-hydroxyethyl)amino]phenyl]ethenyl]-5,5-dimethyl-2-cyclohex-en-1-one (S-3a):

This two step reaction first couples the α, β unsaturated ring-locked bridge unit to the aldehyde donor resulting in extended conjugation and then removes the remaining acetate protecting groups. Two routes are employed. In the case of YLD-124 and JRD1, isophorone is the bridge unit being coupled to S-1a (prepared according to literature methods).[8] The methoxide route outlined below or some variation of the Claisen-Schmidt condensation is sufficent;[3,9-10] however, an alternative route was employed for JRD5 as outlined below.[11]

The condensation reaction can be accomplished quite effectively (conversion up to 90% were observed by ^{1}H-NMR) using sodium metal and methanol. The introduction of sodium metal drives the reaction by eliminating residual water while generating dry methoxide *in-situ*. The reaction is carried out in a dual-neck round bottom flask fitted with a reflux condensor at constant atmospheric pressure under the protection of inert gas with an exterior ice bath. Clean sodium (20 g, 833 mmol) reacts with dry methanol (250- 300 mL) to produce sodium methoxide, hydrogen gas, and heat. The resulting mixture is cloudy and white in color. Isophorone is then added (9.5 mL, 63 mmol) and the solution is heated to reflux under protection of nitrogen. The solution is a dark red color. Dry S-1a is then added (17 g, 58 mmol) and the reaction is refluxed overnight. The resulting mixture must then undergo hydrolysis to completely remove the acetate protecting groups. Residual methanol is removed by rotary evaporation to prepare for simultaneous hydrolysis and liquid-liquid extraction. After rotary evaporation, the dark-red, crude reaction mixture from the previous step is diluted with a large excess of 0.1 N HCl, followed by titration with 1.0 M acetic acid until a sharp color change is observed. The color change presumably marked the point at which the acetate protecting groups were fully removed, a mixture of protected, half protected, and de-protected products was produced when the hydrolysis step was not undertaken (as observed by TLC and NMR). The resulting organic material is extracted from the biphasic mixture in a separatory funnel by minimal aliquots of dichloromethane (DCM) or chloroform, which is then removed under reduced pressure. Further purification can be accomplished by diluting the resulting solids with diethyl ether spiked with 2% to 5% ethyl acetate (EtOAc). The dilution with ether/EtOAc is accompanied by the precipitation of salts (presumably sodium acetate or other sodium based salts) that are conveniently separated using a fritted funnel. Residual salts remaining in the organic layer are then washed away using small aliquots of water or brine. The ether/EtOAc and product mixture is then dried of residual water using magnesium sulfate, and the solvent is removed by rotary evaporation followed by 12 hours in a vacuum oven at 60 °C. The resulting crude organic material can either be further purified by flash column chromatography,[12] precipitation, or crystallization from either EtOAc or acetone. 40% yield. MS (ESI) (M^+H, $C_{20}H_{27}NO_3$): calcd, 330.20 $[M+H]^+$; found, 330.4 $[M+H]^+$.

3-[2-[4-[bis[2-[[(1,1-dimethylethyl)dimethylsilyl]oxy]ethyl]amino]phenyl]-ethenyl]-5,5-dimethyl -2-cyclohexen-1-one (S-4a): Silyl protection is carried out in flame dried glassware by adding *tert*-butyldimethylsilyl chloride (4.0 g, 27 mmol) to mixture of imidazole (2.4 g, 35 mmol) and dry dimethyl formamide (DMF, 9 mL).[9,13] S-3a (2.0 g, 6 mmol) is then added. The reaction is stirred overnight with gentle heating. The reaction is quenched with water, diluted with a mixture of hexanes and EtOAc, and then washed with brine to remove residual DMF and imidazole. Flash chromatography is used to complete the purification and residual solvents are removed by rotary evaporation followed by 12 hours in a vacuum oven at 60 °C.[12,14,15] 99% conversion by TLC, overall yield: 90%.

2-[3-[(1*E*)-2-[4-[bis[2-[[(1,1-dimethylethyl)dimethylsilyl]oxy]ethyl]amino]phenyl]-ethenyl]-5',5'-dimethycyclohex-2-en-1-ylidene]-acetonitrile (S-5a): All glassware is flame dried prior to assembly. A multi-neck round-bottom flask is fitted with a reflux condenser and a stir rod. The flask is charged with 60% sodium hydride suspension (0.2 g, 6 mmol) and placed under the protection of inert gas at a constant one atmosphere of pressure and lowered into an ice bath. Dry, degassed THF is added via syringe (20 mL). Diethyl cyanomethylphosphonate (1.0 mL, 6 mmol) is added drop-wise via syringe producing bubbles of hydrogen gas. The solution is cloudy white. Once the diethyl cyanomethylphosphonate is completely added, the ice bath is removed and the reaction is brought to room temperature. The solution is then clear. Dry S-4a (1.2 g, 2 mmol) is dissolved in dry degassed tetrahydrofuran (THF), then added to the mixture via cannula transfer and the reaction is refluxed overnight.[16-18] The reaction is then cooled, quenched with water, and residual THF is removed by rotary evaporation. The resulting mixture is diluted with a mixture of hexanes and EtOAc. Residual salts are removed via liquid/liquid extraction. The resulting organic layer is dried using magnesium sulfate and flash chromatography is performed. Residual solvent is then removed via rotary evaporation and the product is placed in a vacuum oven at 60 °C overnight to dry. 99% conversion by TLC, 80% yield overall. MS (ESI) (M^+H, $C_{34}H_{56}N_2O_2Si_2$): calcd, 581.39 $[M+H]^+$; found, 581.6 $[M+H]^+$.

2-[3-[2-[4-[bis[2-[[(1,1-dimethylethyl)dimethylsilyl]oxy]ethyl]amino]phenyl]ethenyl]-5,5-dimethyl-2-cyclohexen-1-ylidene]-acetaldehyde (S-6a): A single neck round bottom flask is flame dried and placed under the protection of an inert gas. The flask is charged with pure, dry nitrile (2.3 g, 4 mmol). Dry and degassed toluene is added (100 mL). The reaction vessel is lowered into a bath of dry ice and acetone and allowed to chill. DiBAl-H is added to the mixture drop-wise (6.9 mL, 1 M) and the solution turns a dark red color. The reaction is allowed to react for two hours or monitored by thin layer chromatography (TLC). Hydrolysis is then accomplished by the addition of damp silica (10 g, about 10% water by mass), which is added to the reaction mixture and the reaction is allowed to return to room temperature while being stirred overnight. The resulting mixture is then diluted with hexane/EtOAc, dried with magnesium sulfate, filtered through a coarse grain filter paper, and placed onto a large flash chromatography column. Residual solvent is removed via rotary evaporation and the product is dried in a vacuum oven at 60 °C overnight.[9,19] 58% yield. MS (ESI) (M^+H, $C_{34}H_{57}NO_3Si_2$): calcd, 584.39 $[M+H]^+$; found, 584.7 $[M+H]^+$.

2-[4-(3-{3-[2-(4-{Bis-[2-(*tert*-butyl-dimethyl-silanyloxy)-ethyl]-amino}-phenyl)-vinyl]-5,5-dimethyl-cyclohex-2-enylidene}-propenyl)-3-cyano-5-phenyl-5-trifluoromethyl-5*H*-furan-2-ylidene]-malononitrile (YLD124): A round bottom flask is flame dried, fitted with a reflux condensor, placed under the protection of nitrogen, and charged with dry CF_3-Ph-TCF acceptor (0.4 g, 1 mmol) and aldehyde (0.7 g, 1 mmol). Ethanol is dried with magnesium sulfate and added to the reaction vessel via a filtered syringe. The reaction vessel is lowered into an oil bath and refluxed for 20 minutes. The vessel is then cooled in an ice bath and residual ethanol is removed via rotary evaporation. The resulting mixture is purified using flash column chromatography and precipitation from a concentrated DCM solution in excess cold methanol.[9,19] 20% yield. Desired product was confirmed by TLC, UV-Vis, ESI-MS and ^{1}H NMR and X-ray crystallography.[10]

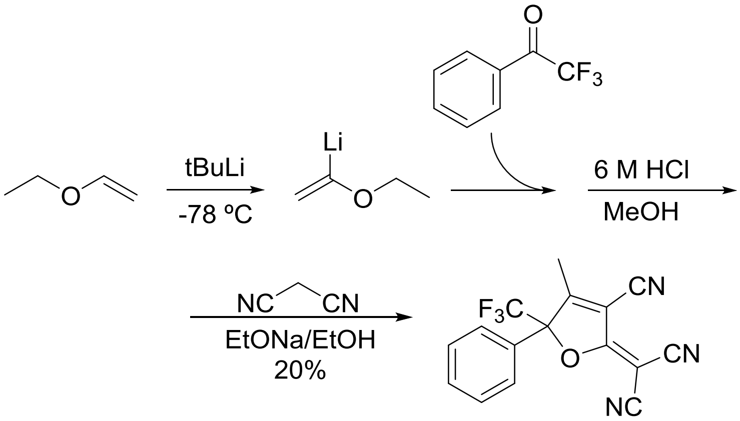

CF$_3$-Ph-TCF

[3-cyano-4-methyl-5-phenyl-5-(trifluoromethyl)-2(5H)-furanylidene]-propanedinitrile (CF$_3$-Ph-TCF Acceptor S-7): CF$_3$-Ph-TCF acceptor was prepared by the application of *tert*-butyl lithium (200 mL 1.7 M (340 mmol) in THF) to ethyl vinyl ether (27.2 mL, 284 mmol) at -78 °C, followed by addition of 2,2,2-trifluoroacetophenone (26.6 mL, 188 mmol) to form the desired ketol, which is then purified by vacuum distillation.[20] 84% yield, GCMS (M$^+$, $C_{10}H_9F_3O_2$): calcd, 218.06; found, 218. The recovered ketol (25 g ketol, 115 mmol) was then condensed with malononitrile (14.9 g, 240 mmol) in a solution of sodium ethoxide in dry ethanol.[21] The resulting solution was condensed via rotary evaporation to remove most of the ethanol, followed by flash chromatography using DCM as the principle solvent. Two distinct fractions were observed, one pale green and one light brown. Both were positive for the desired product by GCMS (M$^+$, $C_{16}H_8F_3N_3O$): calcd, 315.06; found, 315. Further purification was carried out by precipitation of a white powder in cold hexanes. 24% yield.

JRD1:

3-[2-[4-[bis(2-hydroxyethyl)amino]phenyl]ethenyl]-5,5-dimethyl-2-cyclohex-en-1-one (S-3b)*:* Prepared from the synthesis of YLD-124 outlined above.

3-[2-[4-[bis[2-[[(1,1-dimethylethyl)diphenylsilyl]oxy]ethyl]amino]phenyl]-ethenyl]-5,5-dimethyl -2-cyclohexen-1-one (S-4b): *tert*-Butyl(chloro)diphenylsilane (42.5 mL, 163 mmol) was added dropwise to a solution of imidazole (23 g, 337 mmol) and dry DMF (235 mL). S-3b (22.5 g 68.1 mmol) was then added and the reaction was stirred overnight. The resulting mixture was diluted with EtOAc and ether, washed with cold water, dried with sulfates of magnesium and sodium, then purified via flash chromatography and used in the next reaction without further characterization. 90% yield.

2-[3-[(1*E*)-2-[4-[bis[2-[[(1,1-dimethylethyl)diphenylsilyl]oxy]ethyl]amino]phenyl]-ethenyl]-5',5'-dimethycyclohex-2-en-1-ylidene]-acetonitrile (S-5b): Diethyl cyanomethylphosphonate (23.6 mL, 146 mmol) was added dropwise to a solution of sodium hydride suspension (4.9 g, 60% m/m, 123 mmol) in THF. Ice was used to cool the reaction during the addition and then warmed to room temperature and re-submerged into an ice bath for the addition of S-4b. A concentrated solution of S-4b was added via cannula transfer (13.1 g, 16 mmol). The product was identified by TLC and moved to the next reaction without further purification. 90% yield.

2-[3-[2-[4-[bis[2-[[(1,1-dimethylethyl)dimethylsilyl]oxy]ethyl]amino]phenyl]ethenyl]-5,5-dimethyl-2-cyclohexen-1-ylidene]-acetaldehyde (S-6b): A single neck round bottom flask is flame dried and placed under the protection of nitrogen. The flask is charged with S-5b (10 g, 12.1 mmol) and toluene is added. The reaction is chilled with dry ice and acetone. DiBAl-H is added drop-wise. The reaction is allowed to react for two hours. Hydrolysis is then accomplished by addition of damp silica (14.0 g, about 10% water by mass) followed by stirring overnight. Product was identified via TLC (~50% yield), purified via flash chromatography and moved to the final reaction without further characterization. 40% yield overall.

2-[4-(3-{3-[2-(4-{Bis-[2-(*tert*-butyl-diphenyl-silanyloxy)-ethyl]-amino}-phenyl)-vinyl]-5,5-dimethyl-cyclohex-2-enylidene}-propenyl)-3-cyano-5-phenyl-5-trifluoromethyl-5*H*-furan-2-ylidene]-malononitrile (JRD1): The synthesis of JRD1 is essentially identical to that of YLD124. The change in silyl ether protecting group, i.e., the substitution of two methyl groups with two phenyl groups, instills a notable decrease in polarity compared to that of YLD124 which is especially apparent when selecting solvents for thin-layer and flash chromatography. CF_3-Ph-TCF acceptor (3.1 g, 9.8 mmol) and S-6a (6.8 g, 8.1 mmol) are refluxed in ethanol for 20 minutes followed by rotary evaporation and flash chromatography. 34% yield. The desired product is further purified by precipitation overnight from a concentrated solution of DCM into cold excess hexanes. MS (ESI) (M^+, $C_{70}H_{71}F_3N_4O_3Si_2$): calcd, 1128.5011; found, 1128.4998. ^1H NMR δ_H(500 MHz; $CDCl_3$; Me_4Si) 7.61 (8 H, d, J=7.7 Hz, Ar-H), 7.50 (5 H, m, Ar-H), 7.42 (4 H, t, J=7.5 Hz, Ar-H), 7.34 (8 H, t, J=7.4 Hz, Ar-H), 7.18 (2 H, d, J=8.7 Hz, Ar-H), 6.88 (1 H, d, J=15.9 Hz, C-H), 6.72 (1 H, d, J=15.5 Hz, C-H), 6.38 (1 H, s, C-H), 6.31-6.33 (4 H, m, C-H, Ar-H), 3.75 (4 H, t, J=6.1 Hz, C-H_2), 3.50 (4 H, t, J=6.1 Hz, C-H_2), 2.40 (2 H, s, C-H_2), 2.31 (1 H, d, J=16.5 Hz, C-H), 2.22 (1 H, d, J=16.2 Hz, C-H), 1.04 (18 H, s, C-H_3), 1.02 (3 H, s, C-H_3), 0.96 (3 H, s, C-H_3). ^{13}C NMR δ_C(125 MHz; $CDCl_3$; Me_4Si) 175.93, 161.90, 159.19, 152.54, 149.47, 146.60, 136.65, 135.61, 133.28, 131.22, 130.38, 129.94, 129.83, 129.59, 129.56, 128.66, 127.79, 126.76, 125.55, 124.13, 122.22 (Q, $^1J_{CF}$=285 Hz), 115.40, 112.03, 111.86, 111.69, 111.17, 95.67 (Q, $^2J_{CF}$=30.3 Hz), 93.78, 60.86, 56.68, 52.94, 39.89, 39.64, 31.65, 28.62, 28.14, 26.85, 19.11.

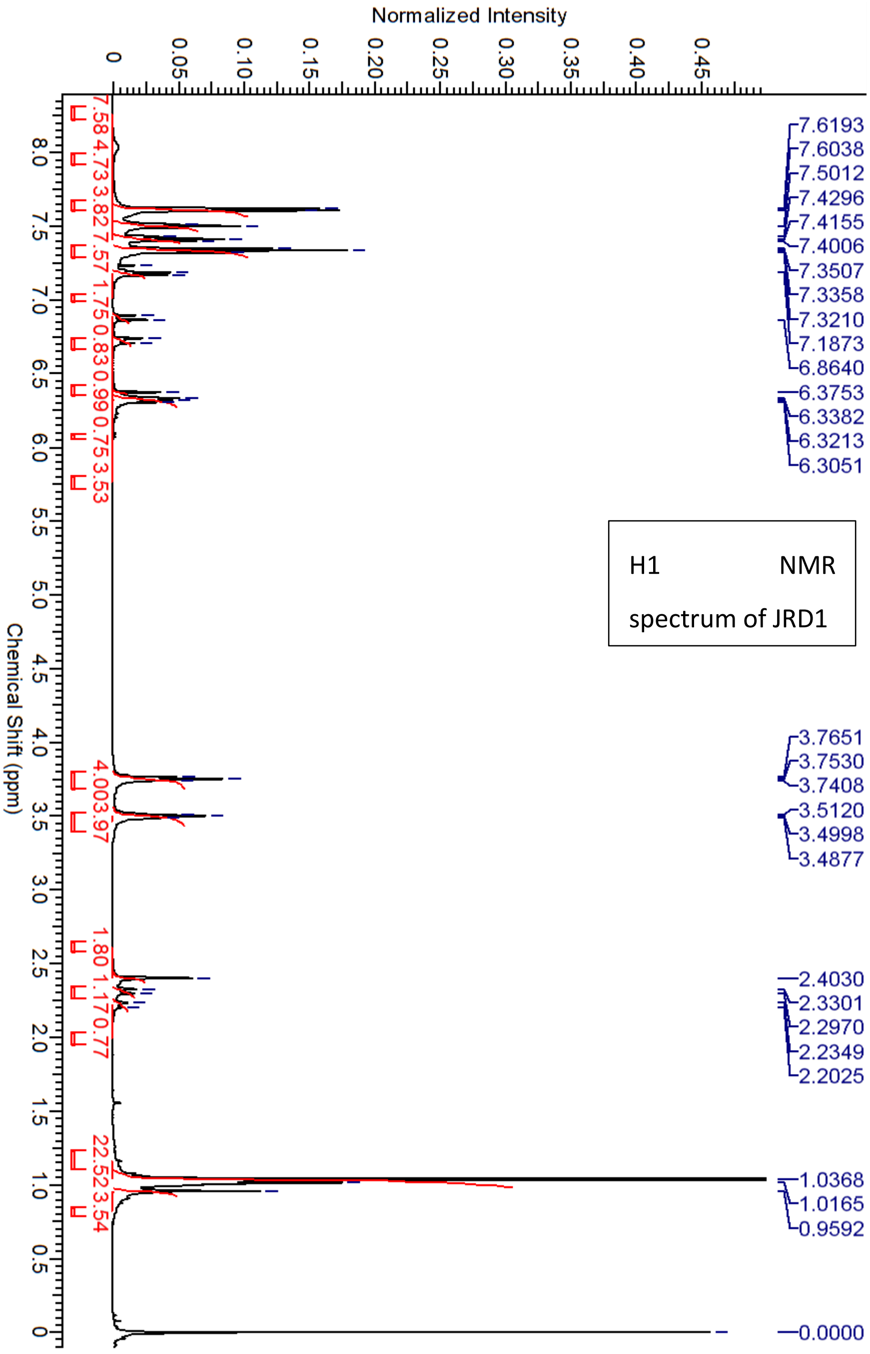

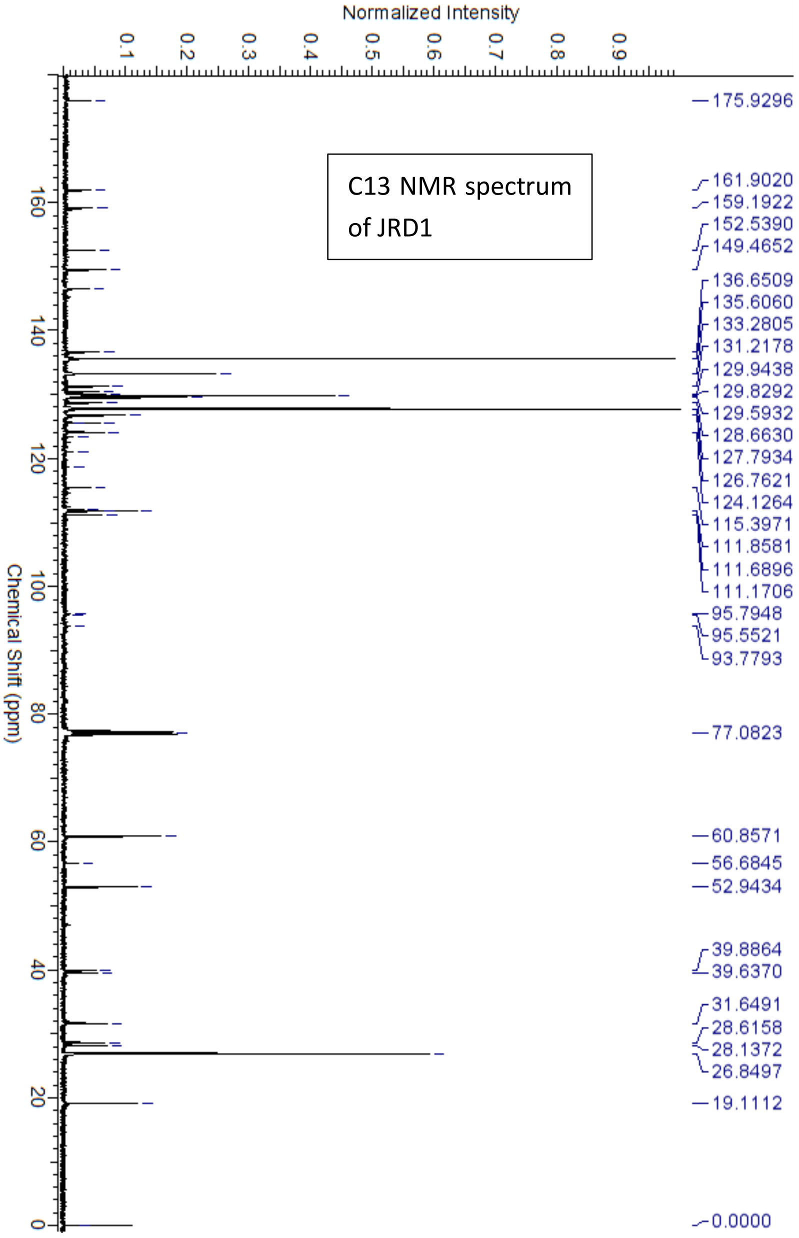

JRD5:

4-{Bis-[2-(*tert*-butyl-diphenyl-silanyloxy)-ethyl]-amino}-benzaldehyde (S-1c): deprotected benzaldehyde (S-1a) was recovered from the synthesis of YLD124 (6.42 g, 31 mmol) and added to a solution of *tert*-butyldimethylsilyl chloride (17.5 mL, 67 mmol) and excess pyridine, then stirred overnight. The reaction was diluted with a mixture of hexanes/ EtOAc and washed with copious amounts of brine, passed through a silica plug, and precipitated in cold methanol. Product was identified by TLC and moved to the next reaction without further purification. Overall yield 90%.

3-[2-(4-{Bis-[2-(*tert*-butyl-diphenyl-silanyloxy)-ethyl]-amino}-phenyl)-vinyl]-2-carbazol-9-yl-5,5-dimethyl-cyclohex-2-enone (S-3c): *Trimethylsilyldiethylammonium route:* An alternative route to condense the bridge unit of JRD5 with the donor was explored.[22] This was in part due to the unpredictability of the sodium methoxide route employed previously, and also to avoid working with sodium metal and harsh reaction conditions that may produce side reactions with the modified bridge. The reaction was carried out by mixing lithium perchlorate (0.72 g, 6 mmol) and *N,N* diethyltrimethylsilylamine (1.9 mL, 10 mmol) and the desired aldehyde (4.9 g, 7 mmol) for ten minutes under nitrogen, followed by addition of the bridge unit. Minimal THF was used as a solvent. The reaction mixture was purified via flash column chromatography and the desired material was identified by TLC. 90% yield.

{3-[2-(4-{Bis-[2-(*tert*-butyl-diphenyl-silanyloxy)-ethyl]-amino}-phenyl)-vinyl]-2-carbazol-9-yl-5,5-dimethyl-cyclohex-2-enylidene}-acetonitrile (S-5c): This reaction was carried out in a manner identical to that pertaining to YLD124 and JRD1 described above. Diethyl cyanomethylphosphonate (6.24 ml, 39mmol) was added to a solution of THF and 60% NaH suspension (1.5 g, 38 mmol). A solution of S-3c (5.0 g, 5 mmol) in THF was then added via cannula transfer and the reaction was refluxed overnight. The reaction was quenched with water and residual THF was removed via rotary evaporation. The resulting mixture was diluted with ethylacetate/hexanes, and residual salts were extracted with cold water. The product was dried with magnesium sulfate and then purified by flash chromatography. Residual solvent was stripped via rotary evaporation followed by 24 hours under vacuum at 60 °C. 90% yield. MS (ESI) (M^+, $C_{66}H_{71}N_3O_2Si_2$): calcd, 1016.50 $[M+Na]^+$; found, 1016.9$[M+Na]^+$.

{3-[2-(4-{Bis-[2-(*tert*-butyl-diphenyl-silanyloxy)-ethyl]-amino}-phenyl)-vinyl]-2-carbazol-9-yl-5,5-dimethyl-cyclohex-2-enylidene}-acetaldehyde: A round bottom flask is charged with S-5c (4.9 g, 5 mmol) and fitted with a reflux condenser. Dry degassed toluene is added (100 mL) and the reaction is cooled to -78 ˚C. DiBAlH in toluene is then added (8.5 mL 1.0 M). The reaction is stirred for 2 hours and monitored by TLC. Damp silica is then added (7 g, 10% water) and the reaction is stirred and allowed to come to room temperature overnight. Product was identified by TLC. 57 % yield.

2-[4-(3-{3-[2-(4-{Bis-[2-(*tert*-butyl-diphenyl-silanyloxy)-ethyl]-amino}-phenyl)-vinyl]-2-carbazol-9-yl-5,5-dimethyl-cyclohex-2-enylidene}-propenyl)-3-cyano-5-phenyl-5-trifluoromethyl-5*H*-furan-2-ylidene]-malononitrile (JRD5) was synthesized as outlined above for YLD124 and JRD1 with additional preparation of the bridge unit and modification of the Claisen-Schmidt condensation step outlined above in the section labeled trimethylsilyldiethylammonium route.[22] CF_3-Ph-TCF acceptor (1.1 g, 3.5 mmol) and S-6a (2.8 g, 2.8 mmol) are refluxed in ethanol for 20 minutes followed by rotary evaporation and column chromatography. 36% yield. MS (ESI) (M^+,

$C_{82}H_{78}F_3N_5O_3Si_2$): calcd, 1293.5590; found, 1293.5604. ^{1}H NMR δ_H(500 MHz; CDCl$_3$; Me$_4$Si) 8.24 (2 H, dd, J=7.8 Hz, 3 Hz), 7.54 (8 H, dd, J=8.1 Hz, 1.4 Hz), 7.38-7.48 (7 H, m), 7.32-7.36 (5 H, m), 7.22-7.30 (10 H, m), 7.05 (2 H, dd, J=8.1 Hz, 4.7 Hz), 6.87 (1 H, d, J=15.9 Hz), 6.53 (2 H, d, J=9.1 Hz), 5.92 (1 H, d, J=14.9 Hz), 5.87 (1 H, d, J=15.9 Hz), 5.77 (2 H, d, J=9.1 Hz), 5.62 (1 H, d, J=12.2), 3.59 (4 H, t, J=6.7 Hz), 3.29 (4 H, t, J=6.6 Hz), 2.75 (2 H, s), 2.66 (1 H, d, J=15.9 Hz), 2.56 (1 H, d, J=15.9 Hz), 1.26 (3 H, s), 1.21 (3 H, s), 0.99 (18 H, s). ^{13}C NMR δ_C(125 MHz; CDCl$_3$; Me$_4$Si) 175.55, 162.54, 153.50, 149.44, 148.92, 146.43, (141.18, 141.14), 138.69, 135.53, 133.13, 131.22, 129.79, 129.73, 129.59, 129.55, 127.72, 126.59, (126.42, 126.33), 124.27, 123.63, (122.95, 122.89), 121.90 (Q, $^1J_{CF}$=285 Hz), 120.52, (120.18, 120.10), 119.68, 116.87, 111.56, 111.32, 111.17, 110.66, 109.92, 95.83 (Q, $^2J_{CF}$=32.0 Hz), 95.58, 60.36, 57.95, 52.71, 40.38, 40.14, 31.02, 28.82, 28.29, 26.78, 19.01.

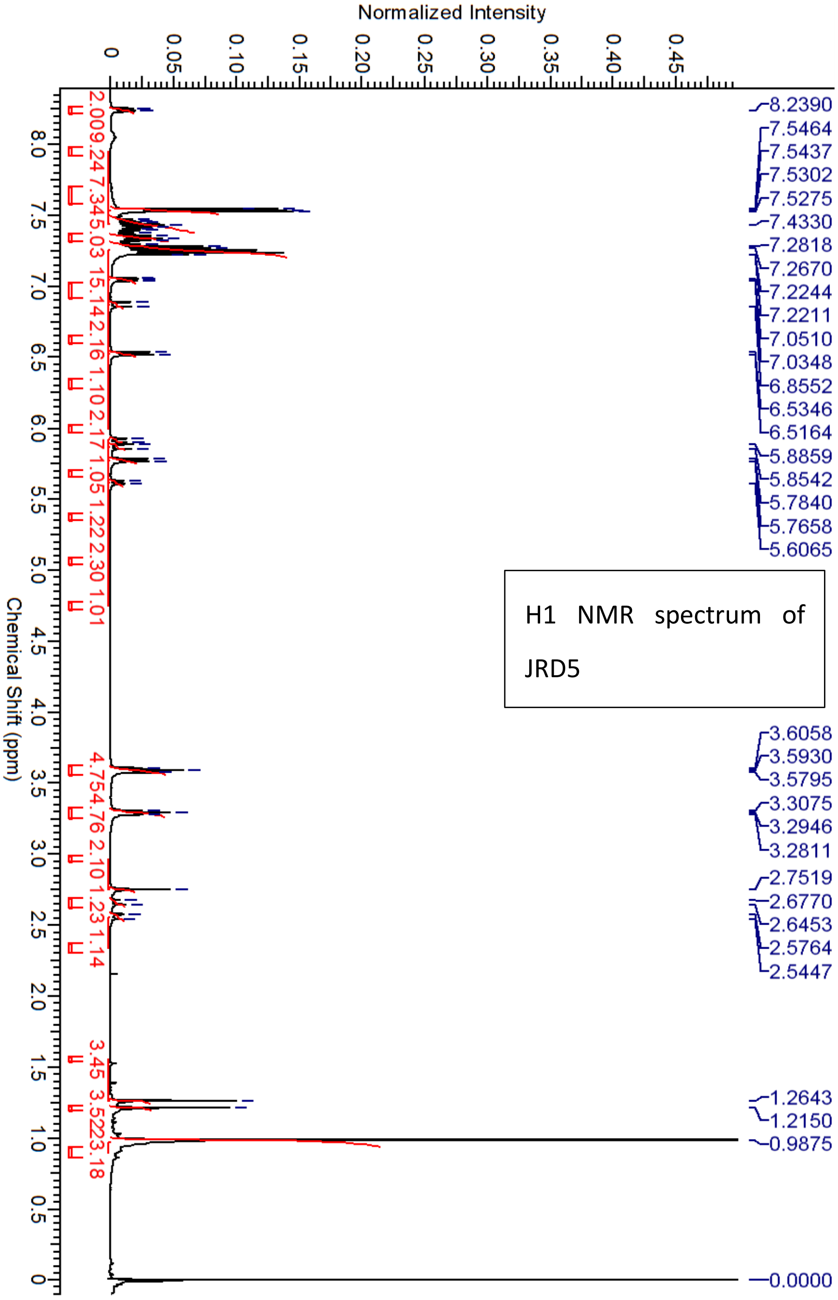

H1 NMR spectrum of JRD5

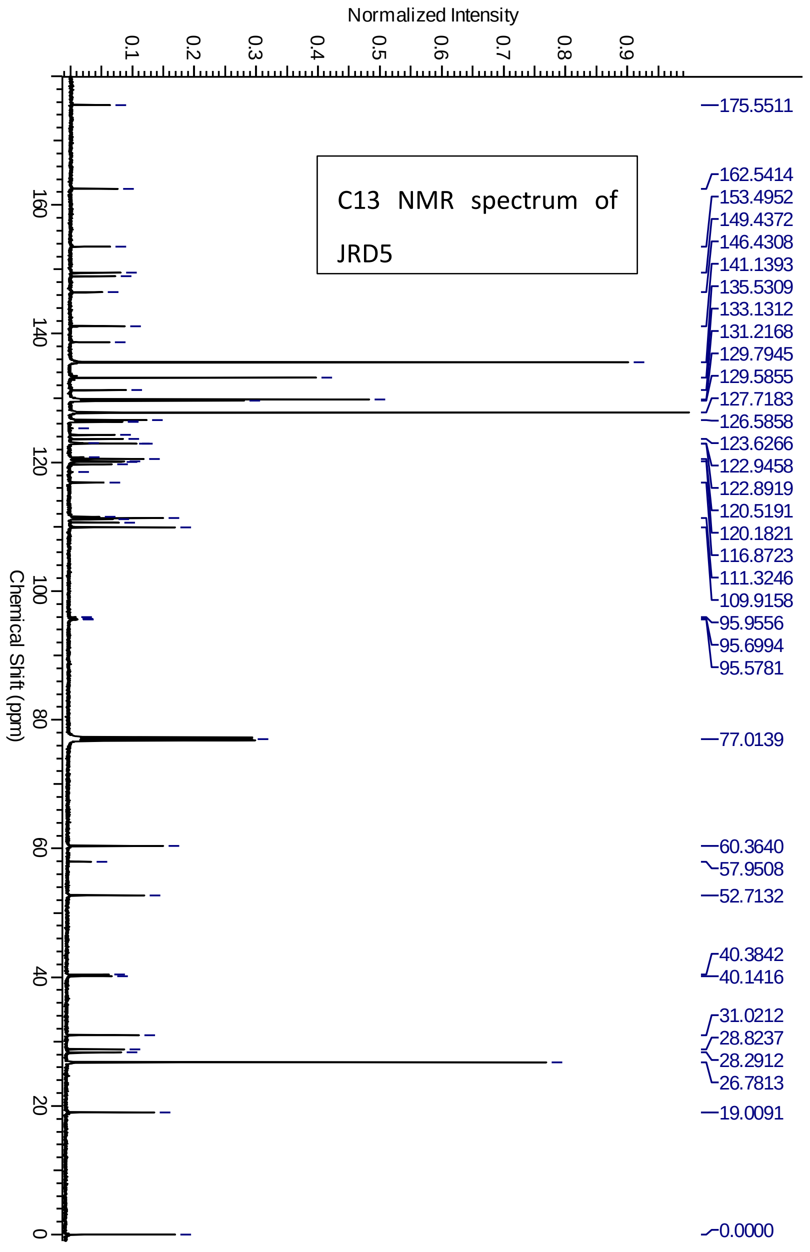

Carbazole-isophorone **S-2b** (**2-(carbazol-9-yl)-3,5,5-trimethylcyclohex-2-en-1-one**):

4-bromoisophorone was prepared according to previously published methods.[9,23,24] SN2' nucleophilic substitution is then carried out to complete the carbazole substituted bridge unit. Carbazole was first purified via recrystallization in ethanol and dried under vacuum. A clean dry round bottom flask is charged with sodium hydride suspension (60%) (6.3 g / 0.26 mol) and THF under the protection of nitrogen at 1 atm constant pressure. The flask is lowered into an ice bath and a solution of slight excess carbazole (29.2 g / 0.17 mol) in THF is added dropwise. Bubbles of hydrogen gas were observed. 4-bromoisophorone (1.0 Meq) was then added and a distinct color change was observed. The reaction was allowed to stir at room temperature overnight. The reaction was quenched with water, diluted with EtOAc, washed with brine in a separatory funnel, dried with magnesium sulfate, and filtered through a fritted funnel. The residual solvent was then removed and via rotary evaporation and the remaining material was purified by flash chromatography and recrystallized in EtOAc.

The major product of the reaction was that of isophorone with carbazole substituted at the 2 position, confirmed by x-ray crystallography (Figure S1). A minor product was also observed by GCMS (Figure S2). The minor product was confirmed to be that resulting from substitution at the 4 position. The minor product was also confirmed via X-ray crystallography, with ambiguous chirality. While the minor product was not reported in previous research, a similar minor peak of identical mass to the primary peak was observed in the gas chromatogram of bridge unit materials used for IKD-1-50.[25]

^{1}H-NMR (300 MHz, $CDCl_3$): δ 8.108 (d, J = 7.8, 2 H), 7.386 (t, J = 7.6, 2 H), 7.239 (t, J = 7.2, 2 H), 7.000 (d, J=8.0, 2H), 2.652 (s, 2 H), 2.591 (s, 2 H), 1.724 (s, 3 H), 1.291 (s, 6 H). ^{13}C-NMR (125 MHz, $CDCl_3$): δ 193.937, 159.503, 140.870, 130.454, 126.123, 126.055, 123.519, 120.779, 120.631, 119.975, 119.781, 109.769, 109.675, 51.845, 46.732, 33.360, 28.651, 20.893.

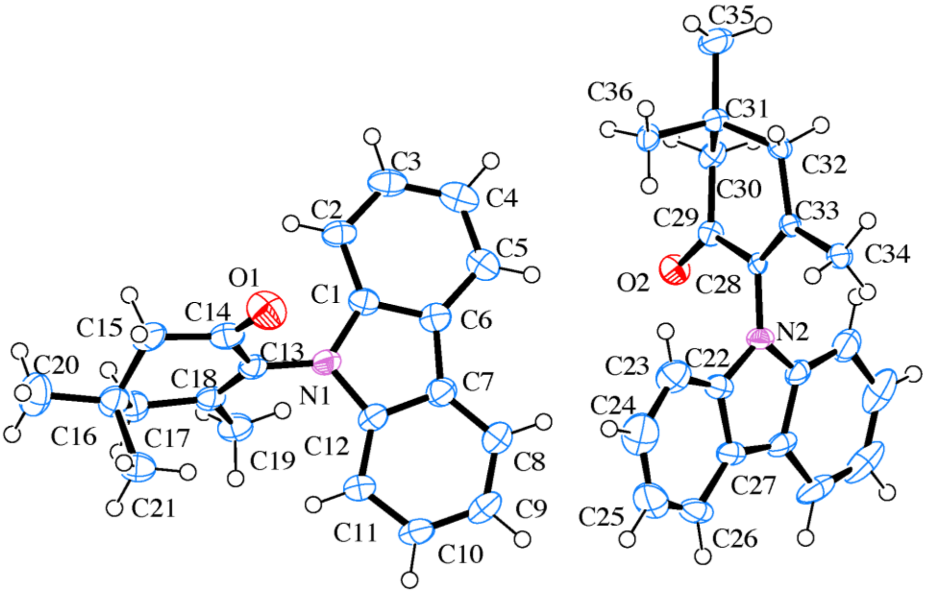

Figure S1. Crystal Structure of JRD5 Bridge Unit.

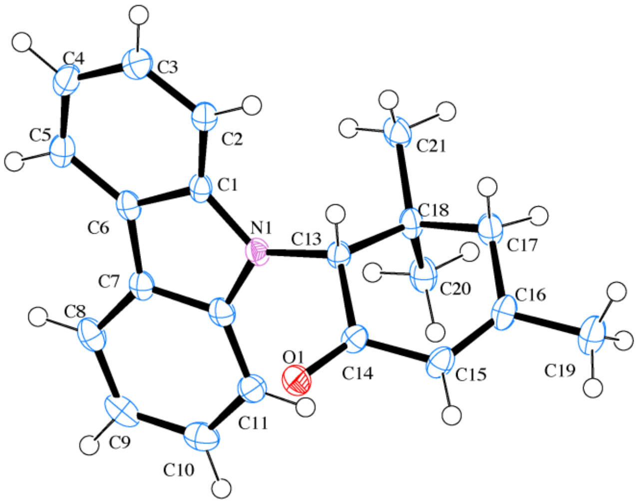

Figure S2. Crystal Structure of JRD5 Bridge Unit (Minor Product).

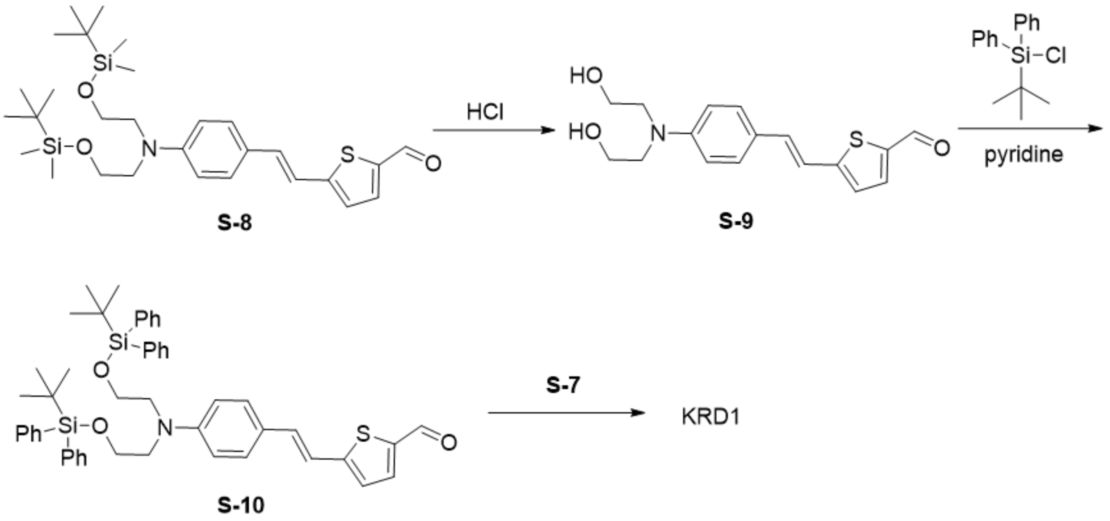

KRD1:

2-[4-(2-{5-[2-(4-{Bis-[2-(*tert*-butyl-diphenyl-silanyloxy)-ethyl]-amino}-phenyl)-vinyl]-thiophen-2-yl}-vinyl)-3-cyano-5-phenyl-5-trifluoromethyl-5*H*-furan-2-ylidene]-malononitrile. KRD1 was synthesized from precursor materials (aldehyde S-8) previously prepared for YLD156.[26] Hydrolysis of the *tert*-butyl dimethyl silyl protecting groups was followed by re-protection with that of diphenyl. Condensation of S10 (1.4 g, 1.7 mmol) with the CF_3-Ph-TCF acceptor (0.6 g, 1.9 mmol) was then carried out by reflux in ethanol for 20 minutes. Desired product was purified by flash chromatography. Yield 38%. MS (ESI) (M^+, $C_{65}H_{61}F_3N_4O_3SSi_2$): calcd, 1090.3950; found, 1090.3934. ^{1}H NMR δ_H(300 MHz; $CDCl_3$; Me_4Si) 7.77 (1 H, d, J=15.1 Hz, C-H), 7.62 (8 H, d, J=6.5 Hz, Ar-H), 7.55-7.52 (5 H, m, Ar-H), 7.43 (4 H, t, J=7.3 Hz, Ar-H), 7.35 (8 H, t, J=6.9 Hz, Ar-H), 7.30 (1 H, d, J=4.2 Hz, C-H), 7.17 (2 H, d, J=8.9 Hz, Ar-H), 7.07 (1 H, d, J=15.7 Hz, C-H), 7.01 (1 H, d, J=4.1 Hz, C-H), 6.93 (1 H, d, J=15.7 Hz, C-H), 6.60 (1 H, d, J=15.3 Hz, C-H), 6.30 (2 H, d, J=8.9 Hz, Ar-H), 3.75

(4 H, t, J=5.9 Hz, C-H$_2$), 3.50 (4 H, t, J=5.9 Hz, C-H$_2$), 1.04 (18 H, s, C-H$_3$). ^{13}C NMR δ_C(125 MHz; CDCl$_3$; Me$_4$Si) 175.31, 162.05, 157.27, 149.40, 143.74 141.75, 137.98, 136.38, 135.57, 133.24, 131.57, 129.80, 129.61, 129.26, 127.75, 127.53, 126.83, 123.17, 115.5, 111.79, 111.67, 111.04, 110.61, 96.85, 96.70, 60.76, 58.34, 52.90, 26.81, 19.07 (CF$_3$ carbon too weak to observe).

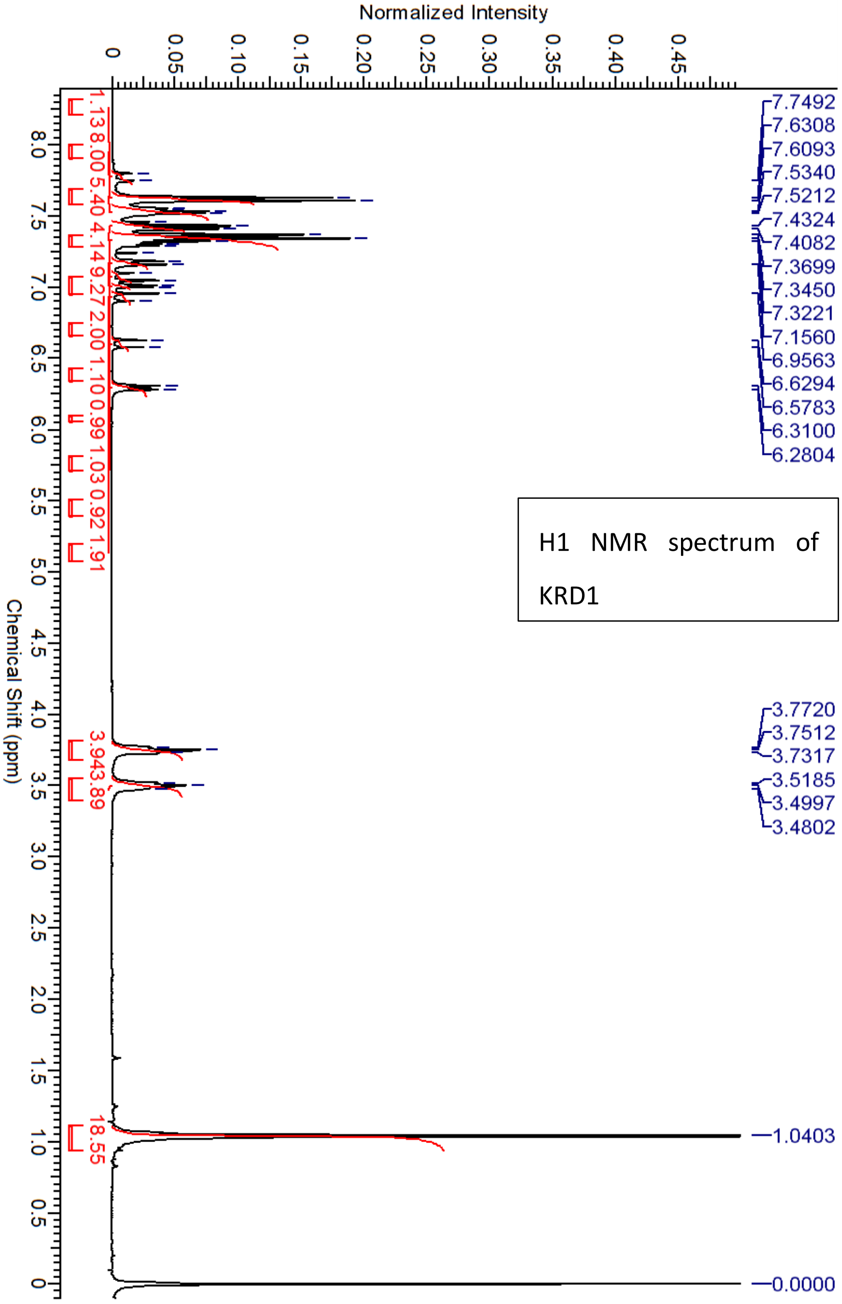

H1 NMR spectrum of KRD1

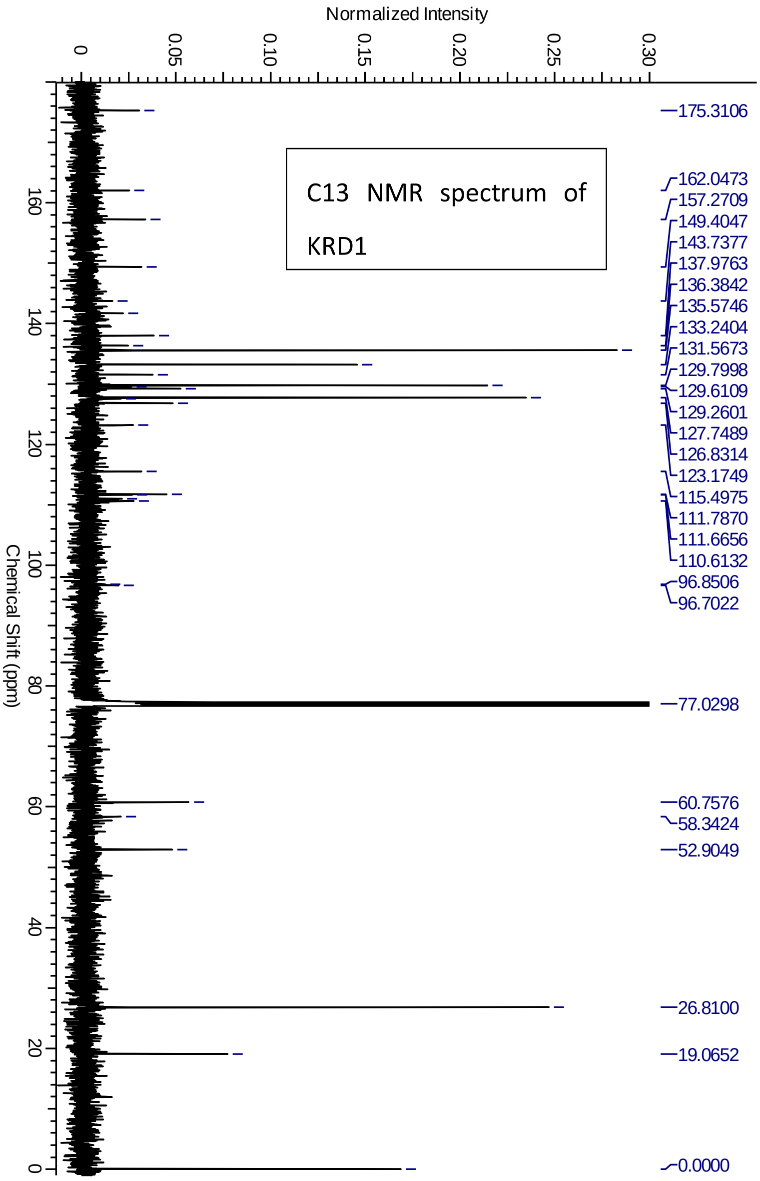

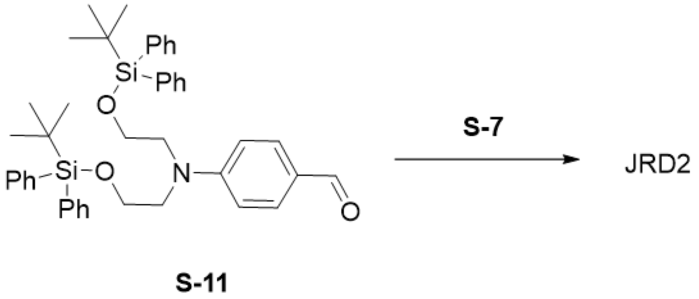

JRD2:

2-{4-[2-(4-{Bis-[2-(*tert*-butyl-diphenyl-silanyloxy)-ethyl]-amino}-phenyl)-vinyl]-3-cyano-5-phenyl-5-trifluoromethyl-5*H*-furan-2-ylidene}-malononitrile. JRD2 was recovered as a byproduct of the synthesis of JRD1. Test reactions confirmed that the product could be synthesized through condensation of CF_3-Ph-TCF acceptor and the corresponding donor. MS (ESI) (M^+, $C_{59}H_{57}F_3N_4O_3Si_2$): calcd, 983.3994 $[M+H]^+$; found, 983.3977 $[M+H]^+$. ^1H NMR δ_H(300 MHz; $CDCl_3$; Me_4Si) 7.69 (1 H, d, J=15.3 Hz, C-H), 7.52-7.58 (12 H, m, Ar-H), 7.38-7.43 (5 H, m, Ar-H), 7.30-7.34 (8 H, m, Ar-H), 7.21 (2 H, d, J=9.0 Hz, Ar-H), 6.69 (1 H, d, J=15.3 Hz, C-H), 6.39 (2 H, d, J=9.0 Hz, Ar-H), 3.77 (4 H, t, J=5.4 Hz, C-H_2), 3.55 (4 H, t, J=5.7 Hz, C-H_2), 1.02 (18 H, s, C-H_3). ^{13}C NMR δ_C(125 MHz; $CDCl_3$; Me_4Si) 175.99, 163.01, 153.65, 151.08, 135.49, 134.78, 132.84, 131.32, 130.14, 129.92, 129.61, 127.8, 127.68, 126.84, 122.55, 112.72, 111.5, 111.06, 108.71, 96.05 (Q, $^2J_{CF}$=30.4 Hz), 94.13, 60.69, 56.71, 53.07, 26.77, 19.02, (CF_3 carbon too weak to observe).

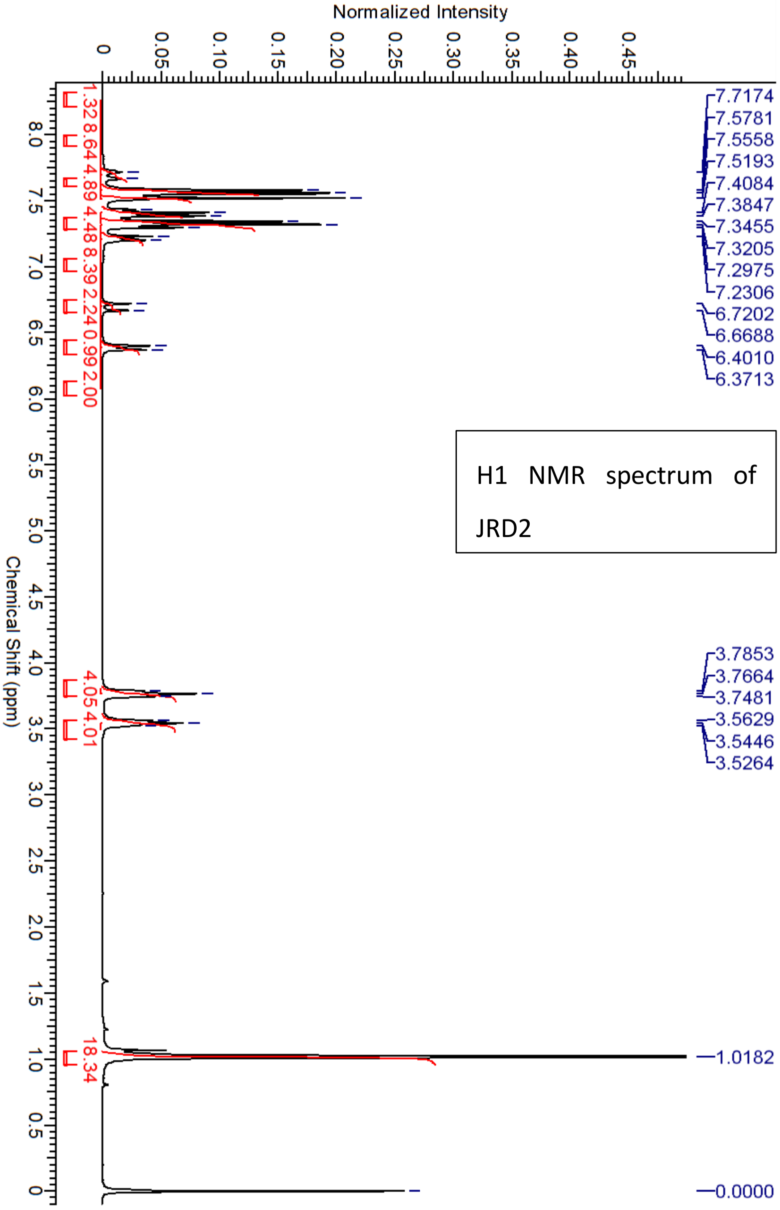

H1 NMR spectrum of JRD2

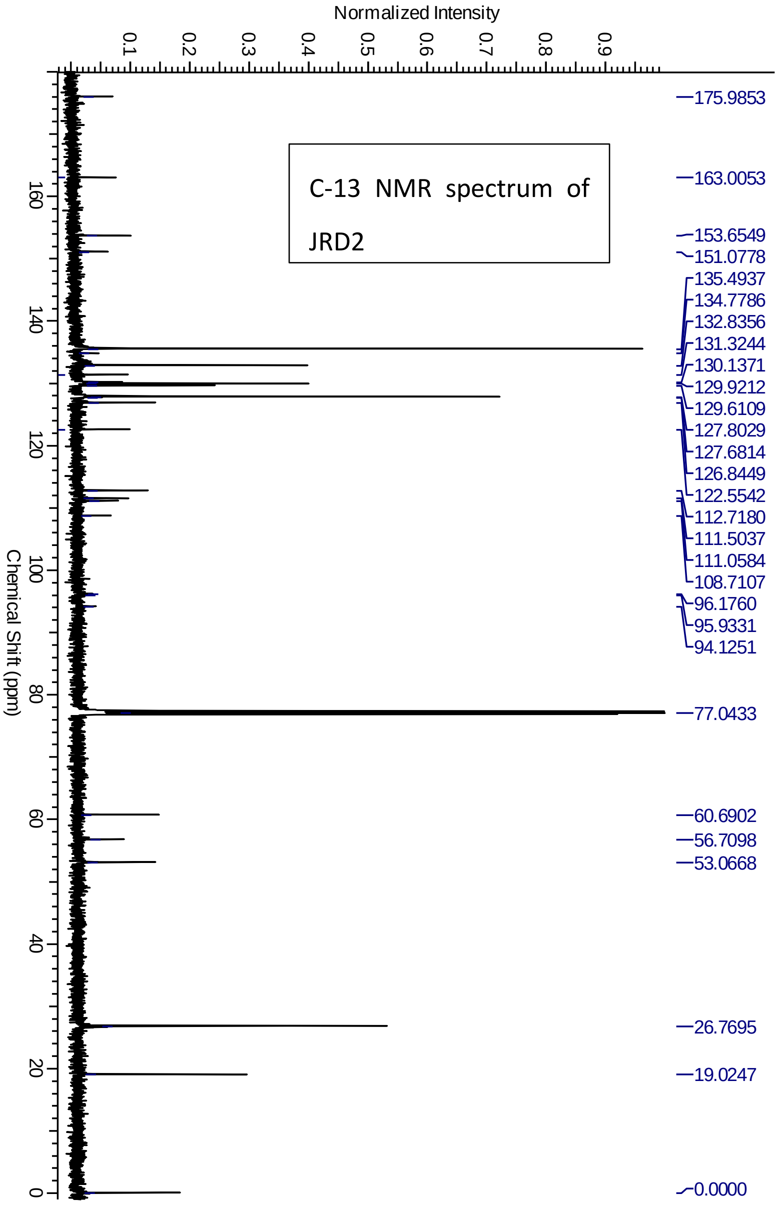

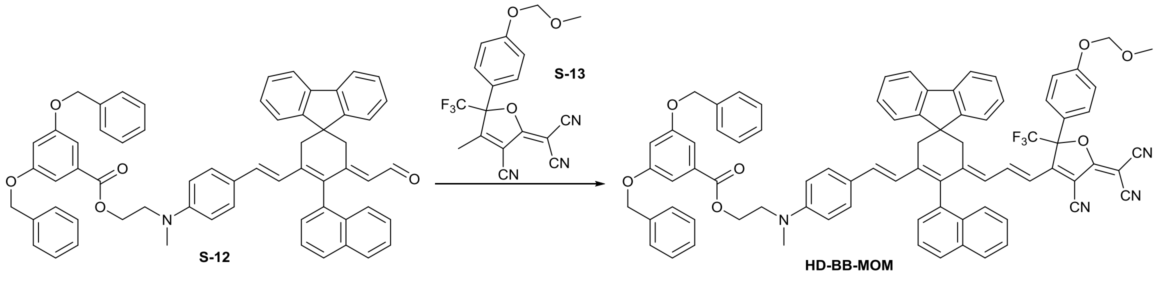

2-({4-[(E)-2-[(5*E*)-5-[(2*E*)-3-[4-cyano-5-(dicyanomethylidene)-2-[4-(methoxymethoxy)phenyl]-2-(trifluoromethyl)-2,5-dihydrofuran-3-yl]prop-2-en-1-ylidene]-4-(naphthalen-1-yl)spiro[cyclohexane-1,9'-fluoren]-3-en-3-yl]ethenyl]phenyl}(methyl)amino)ethyl 3,5-bis(benzyloxy)benzoate (**HD-BB-MOM**): Aldehyde **S-12** (4.1 g, 4.6 mmol, orange solid) and acceptor **S-13** (2.60 g, 6.93 mmol, light green powder) were charged to a flask, purged with nitrogen, and 12.0 mL ethanol was added. After heating to 70°C for 10 min, solubility was not very good, so 8 mL chloroform was added and heating under nitrogen was resumed for 2 hr resulting in a dark green solution. Solvent was stripped off by rotovap, and the product was purified by silica gel chromatography using gradient elution from 100% DCM to 15:1 DCM: EtOAc. Yield = 5.16 g (90%). HRMS (ESI) (M^+ $C_{80}H_{61}F_3N_4O_7$): calcd, 1246.4492; found, 1246.4463. δ_H(300 MHz; $CDCl_3$; Me_4Si) 8.03 (2 H, m), 7.86 (2 H, m), 7.43-7.72 (11 H, m), 7.28-7.39 (10 H, m), 7.16 (2 H, d, J=2.4 Hz), 7.12 (2 H, dd, J=8.8 Hz, J=2.4 Hz), 6.90 (1 H, d, J=9.0 Hz), 6.85 (2 H, d, J=8.8 Hz), 6.79 (1 H, d, J=9.2 H), 6.77 (1 H, t, J=2.4 Hz), 6.65 (1 H, br d, J=15.9 Hz), 6.52 (2 H, d, J=9.0 Hz), 6.37 (1 H, dd, J=15.5 Hz, J=3.5 Hz), 5.99 (1 H, dd, J=14.7 Hz, J=7.9 Hz), 5.92 (1 H, dd, J=12.3 Hz, J=5.9 Hz), 5.14 (1 H, s), 5.07 (1 H, s), 4.97 (4 H, s), 4.37 (2 H, t, J=5.7 Hz), 3.65 (2 H, t, J=5.5 Hz), (3.49, 3.48) (3 H, s), 3.35 (1 H, dd, J=18.0 Hz, J=5.3 Hz), 3.22 (1 H, dd, J=31.7 Hz, J=17.3 Hz), 2.99 (1 H, dd, J=18.2 Hz, J=9.0 Hz), 2.95 (3 H, s), 2.77 (1 H, dd, J=24.0 Hz, J=15.8 Hz).

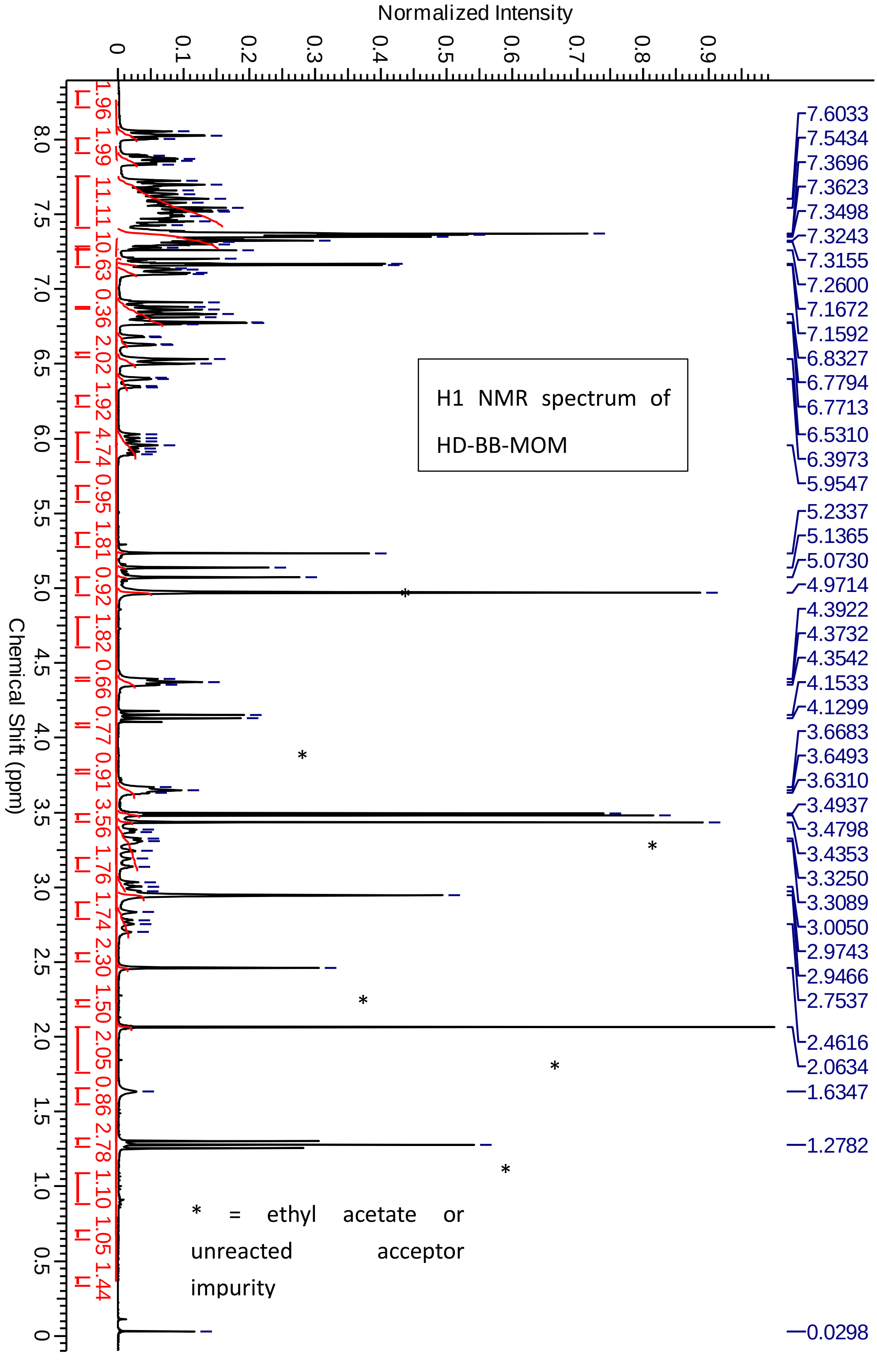

H1 NMR spectrum of HD-BB-MOM

* = ethyl acetate or unreacted acceptor impurity

UV-visible Absorbance Spectra:

UV-visible absorbance spectra were measured from both the chloroform solution and thin films for the series of chromophores studied herein. The solution phase absorbance spectra (Figure S3) for YLD-124 and JRD1 in chloroform are nearly identical; the main absorption bands are at 786 nm and 788 nm, respectively. Molecular substitution at the bridge led JRD5 to a slight hypsochromic shift from that of YLD-124 and JRD1. In general, λ_{max} for YLD-124, JRD1 and JRD5 in chloroform solution are very similar. However, bridge size and types showed great influence on the optical properties. The absorbance spectra of KRD1, the chromophore with a thiophene bridge, showed hypsochromic shift compared to that of JRD5. Without a bridge, the main absorption band for JRD2 further hypsochromic shifted to 630 nm. Figure S4 shows UV-vis spectra as a dependence of the molar absorptivity (ε) on the wavelength in chloroform. The normalized thin film absorbance spectra are shown in Figure S5. The tendency of the absorption behavior is similar in thin films as in the solution.

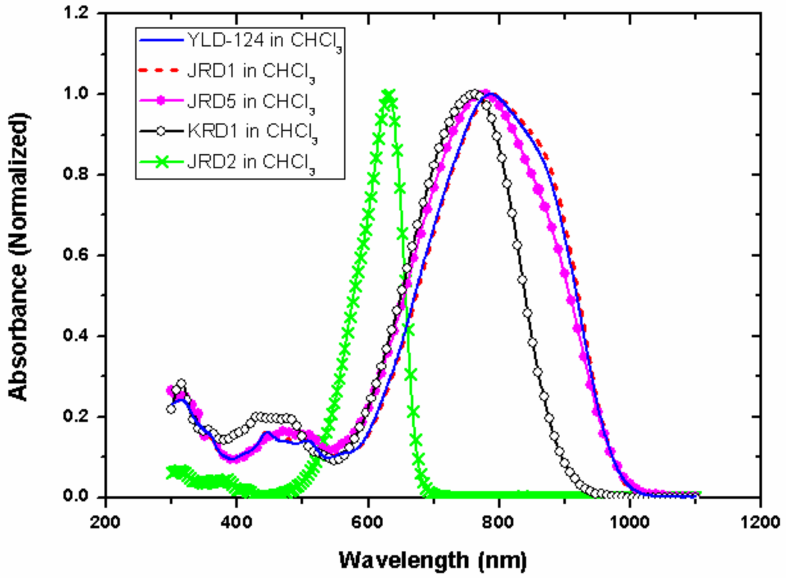

Figure S3. Normalized UV-vis spectra in chloroform for YLD-124 (blue solid line), λ_{max} = 786 nm; JRD1 (red dash line), λ_{max} = 788 nm; JRD5 (magenta triangles), λ_{max} = 778 nm; KRD1 (black circles), λ_{max} = 762 nm; and JRD2 (green crosses), λ_{max} = 630 nm.

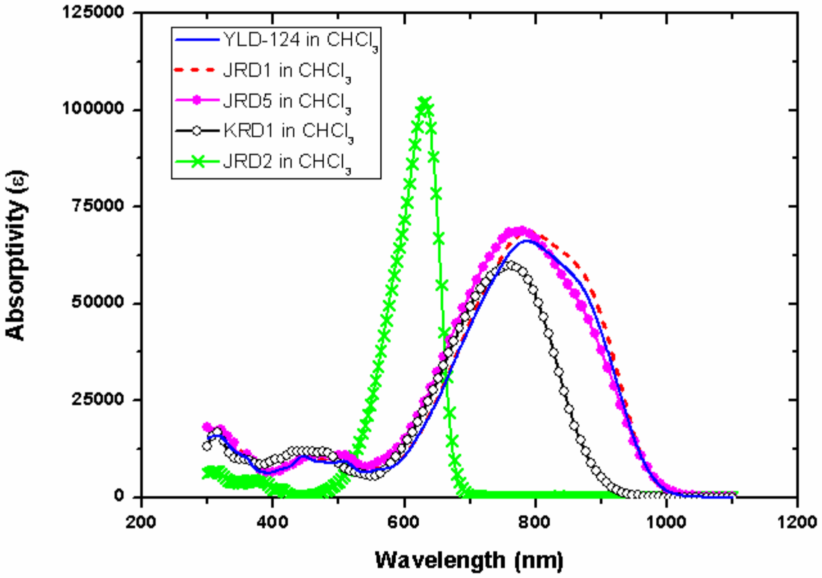

Figure S4 UV-vis spectra as a dependence of the molar absorptivity (ε) in chloroform for YLD-124 (blue solid line), ε = 6.61 × 10^4; JRD1 (red dash line), ε = 6.89 × 10^4; JRD5 (magenta triangles), ε = 6.86 × 10^4; KRD1 (black circles), ε = 5.98 × 10^4; and JRD2 (green crosses), ε = 1.02 × 10^5.

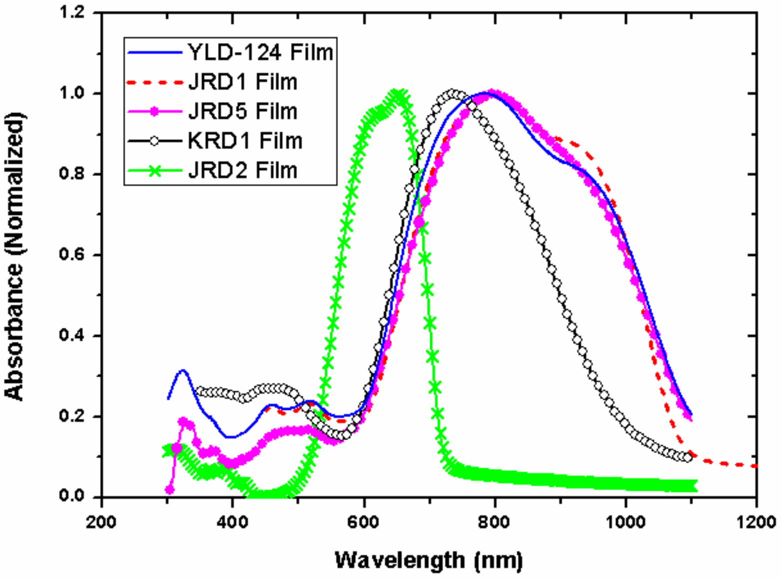

Figure S5. Normalized UV-vis thin film spectra for YLD-124 (blue solid line), λ_{max} = 783 nm; JRD1 (red dash line), λ_{max} = 800 nm; JRD5 (magenta triangles), λ_{max} = 795 nm; KRD1 (black circles), λ_{max} = 737 nm; and JRD2 (green crosses), λ_{max} = 652 nm.

Glass Transition Temperatures

Glass transition temperature (T_g) was measured by Differential Scanning Calorimetry (DSC). A three cycle heat/cool loop was run for each sample under nitrogen at a rate of 10 °C /minute from 0 °C to 150 °C, 0 °C to 180 °C, and 0 °C to just under the temperature of decomposition using a TA Instruments Q100 calorimeter with a refrigerated cooling system (RCS). Data were analyzed using TA Instruments Universal Analysis software.

Without a polymer host, the T_g values for YLD-124 and JRD1 reduced to 81 °C and 82 °C, respectively, which agrees well with other neat chromophores reported so far.[27-29] This is an disadvantage for neat chormophores in applications since T_g is tightly related to the thermal stability. However, the T_g of JRD5 gained a remarkable increase to 101 ˚C, which is comparable to the guest/PMMA material system. Such increase could be attributed to the large, rigid, fused ring moiety carbazole introduced to the bridge for reducing the possibility of lowering T_g due to the additional chromophore substituents with high flexibility and many degrees of rotational freedom. This exploration opens a new avenue to increase T_g for the neat materials with incredible EO performance and calls for further studies. Figure S6-S10 shows the DSC plot of this series of chromophores. Figure S11 shows the DSC plot of the comparative choromophore HD-BB-MOM.

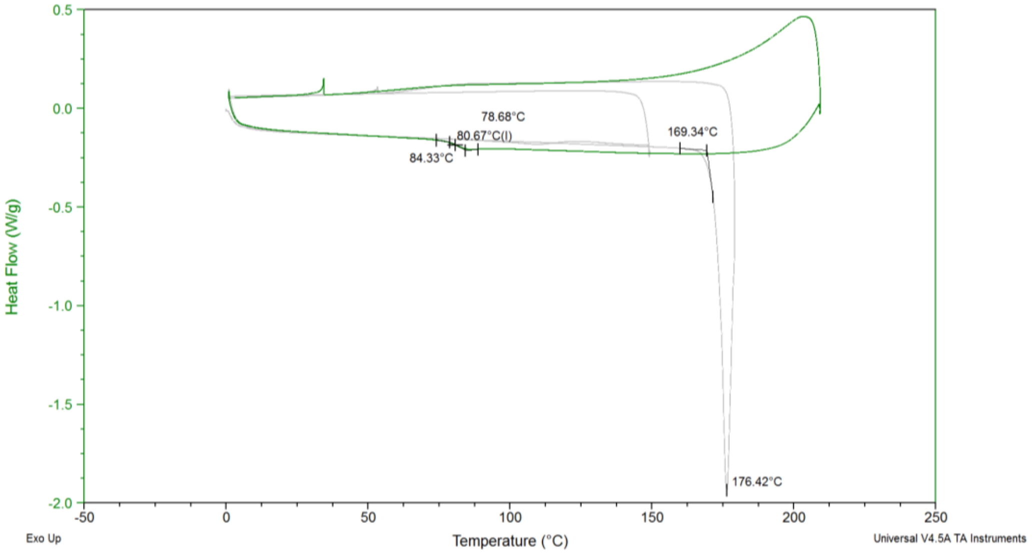

Figure S6. DSC plot of YLD-124. T_g = 80.67 °C.

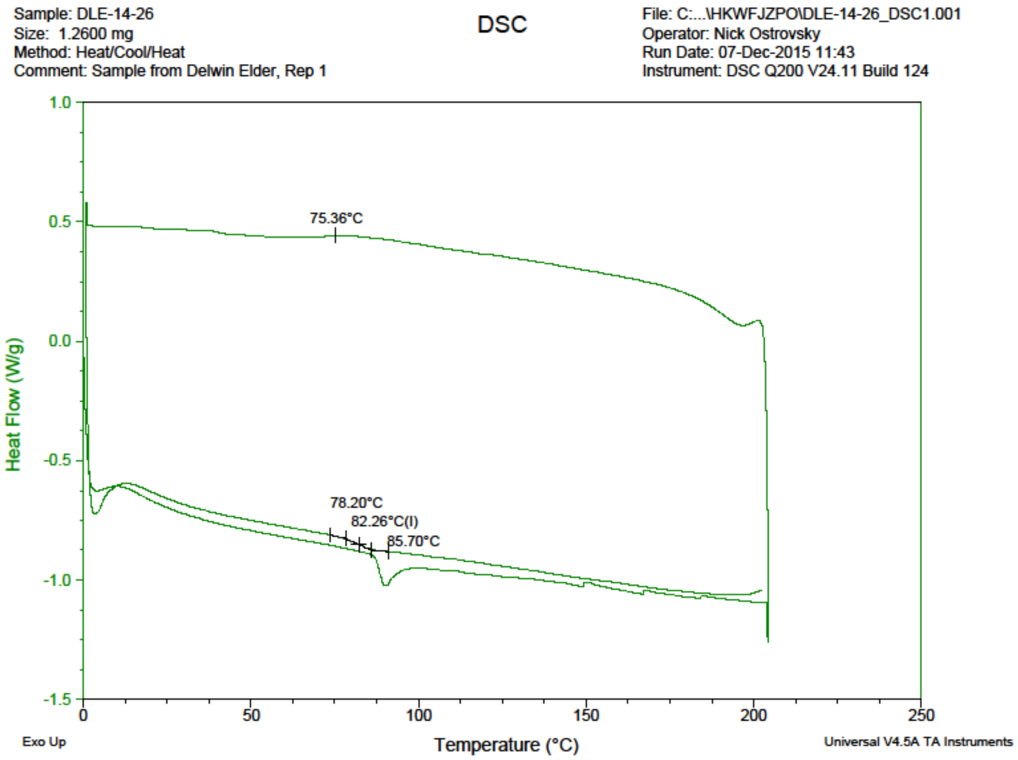

Figure S7. DSC plot of JRD1. T_g = 82.26 °C.

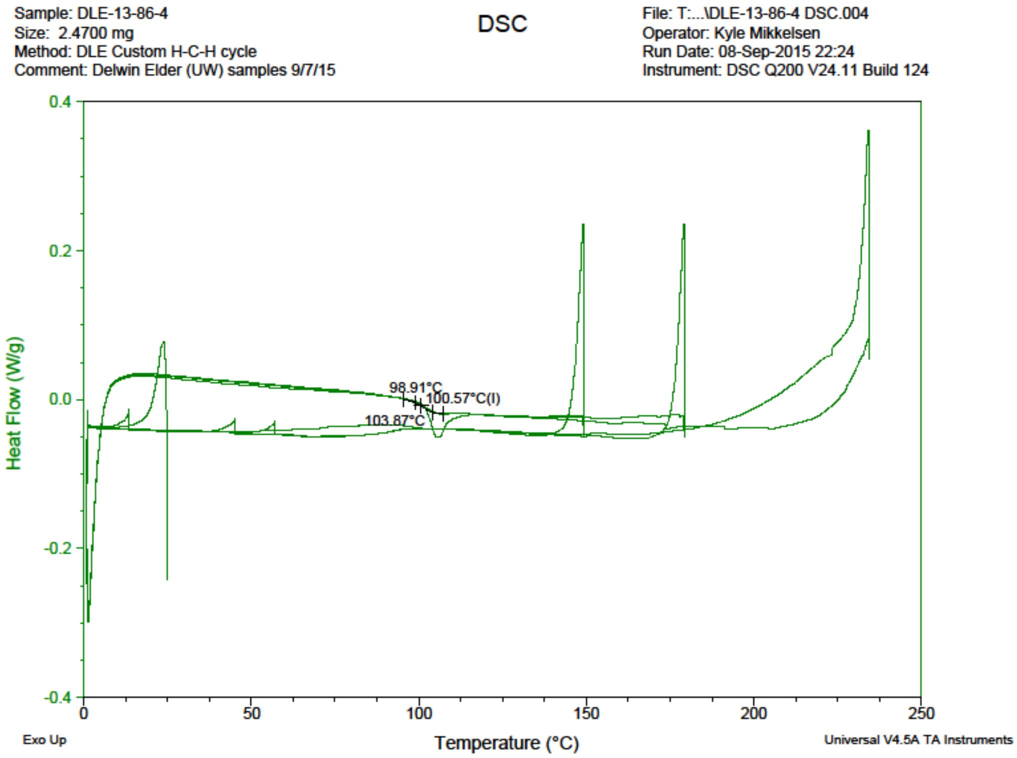

Figure S8. DSC plot of JRD5. T_g = 100.57 °C.

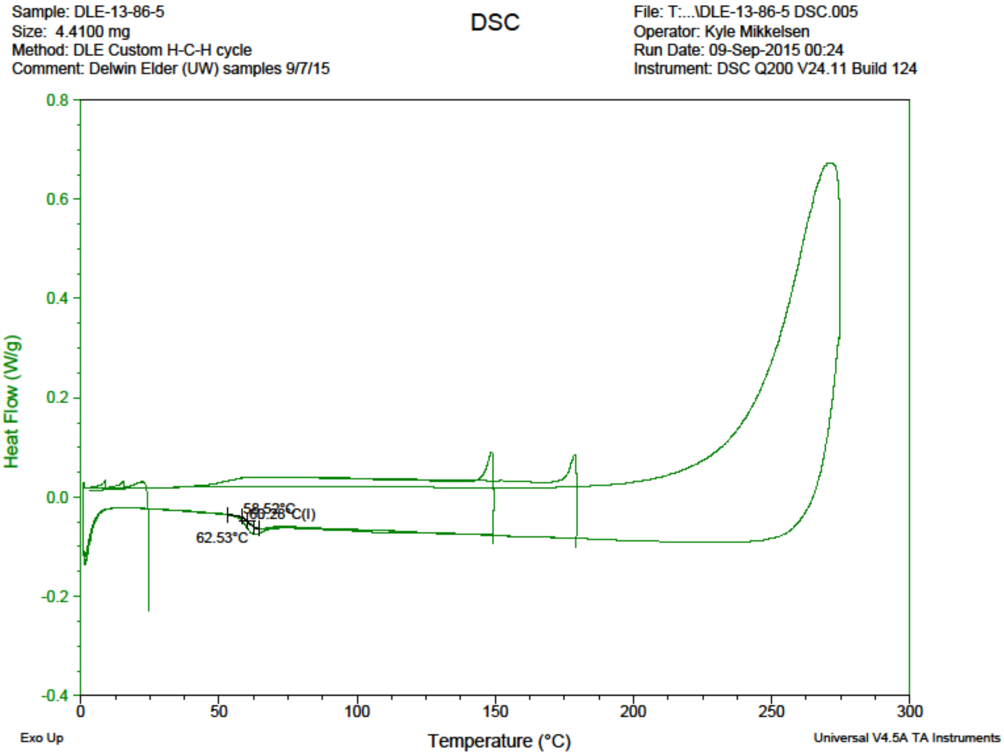

Figure S9. DSC plot of JRD2. T_g = 60.28 °C.

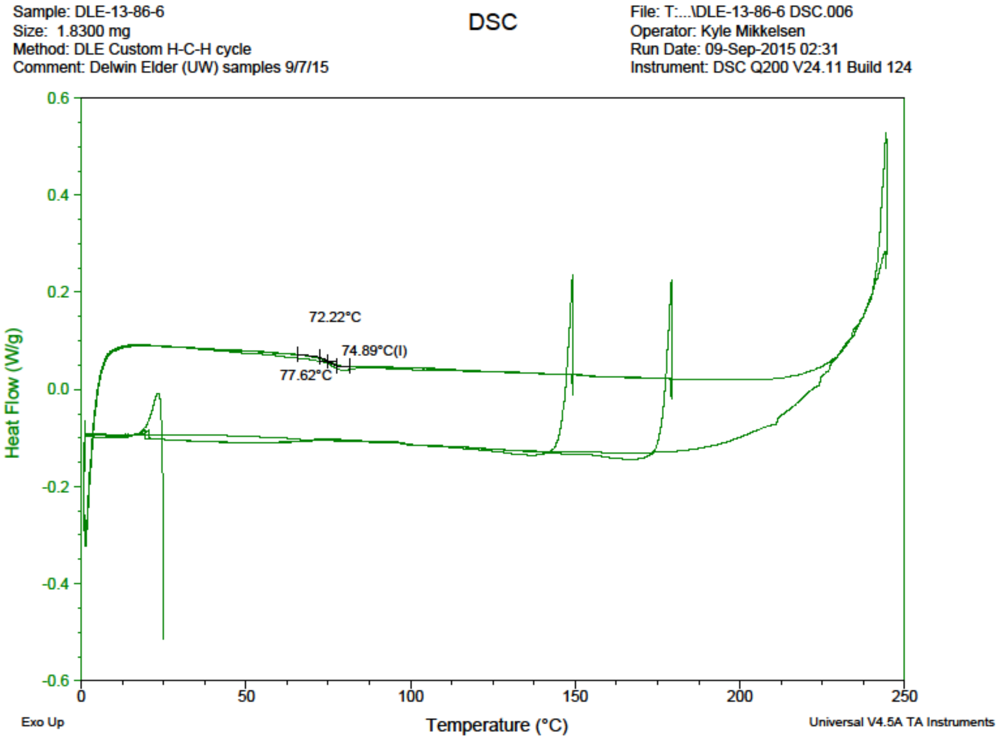

Figure S10. DSC plot of KRD1. T_g = 74.89 °C.

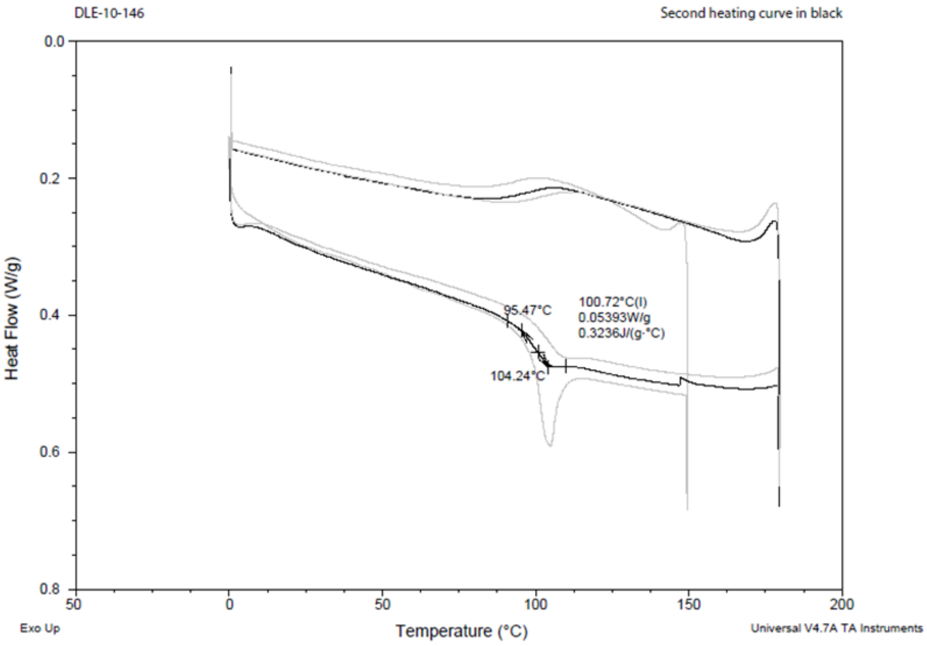

Figure S11. DSC plot of HD-BB-MOM. T_g = 100.72 °C.

The Decomposition Temperature

The decomposition temperatures (T_d) was measured by thermogravametric analysis (TGA). Thermogravimetric analysis (TGA) samples were prepared by placing over 1 mg of sample onto a platinum TGA pan. The samples were scanned at a rate of 20 °C/minute from room temperature up to 400 °C.

The T_d of YLD-124 is 208 °C. The other four chromophores have increased T_d compared to that of YLD-124. The T_d of JRD1, JRD5, JRD2 and KRD1 is 226.18 °C, 233.07 °C, 271.82 °C, and 239.87 °C, respectively.

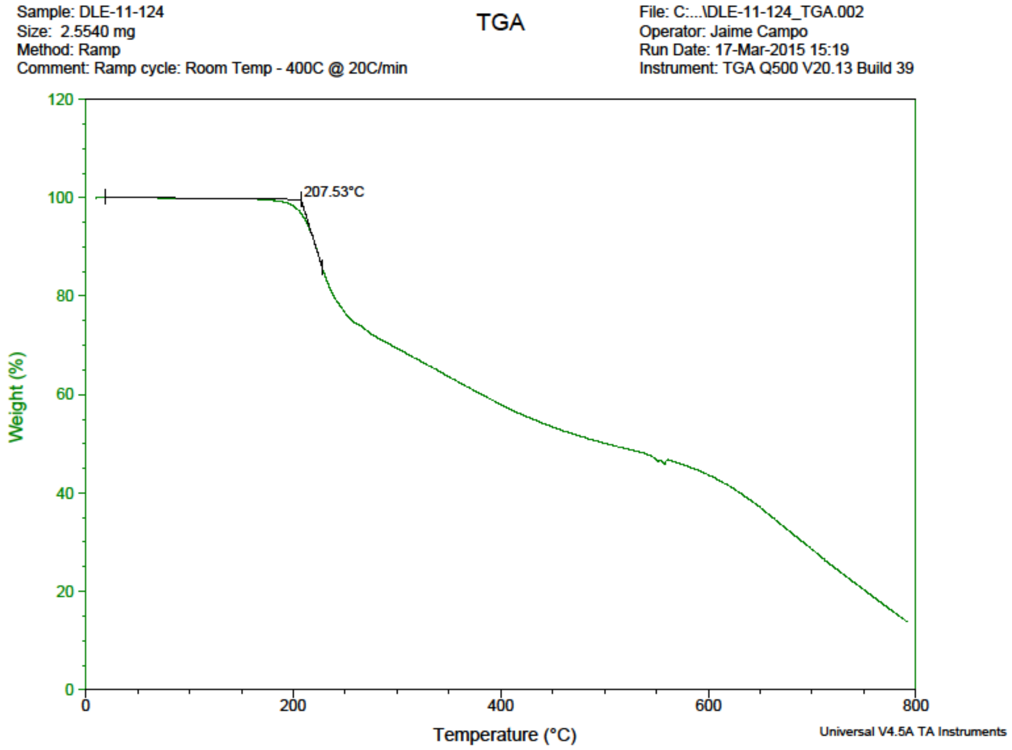

Figure S12. TGA plot of YLD-124. T_d=207.53 °C.

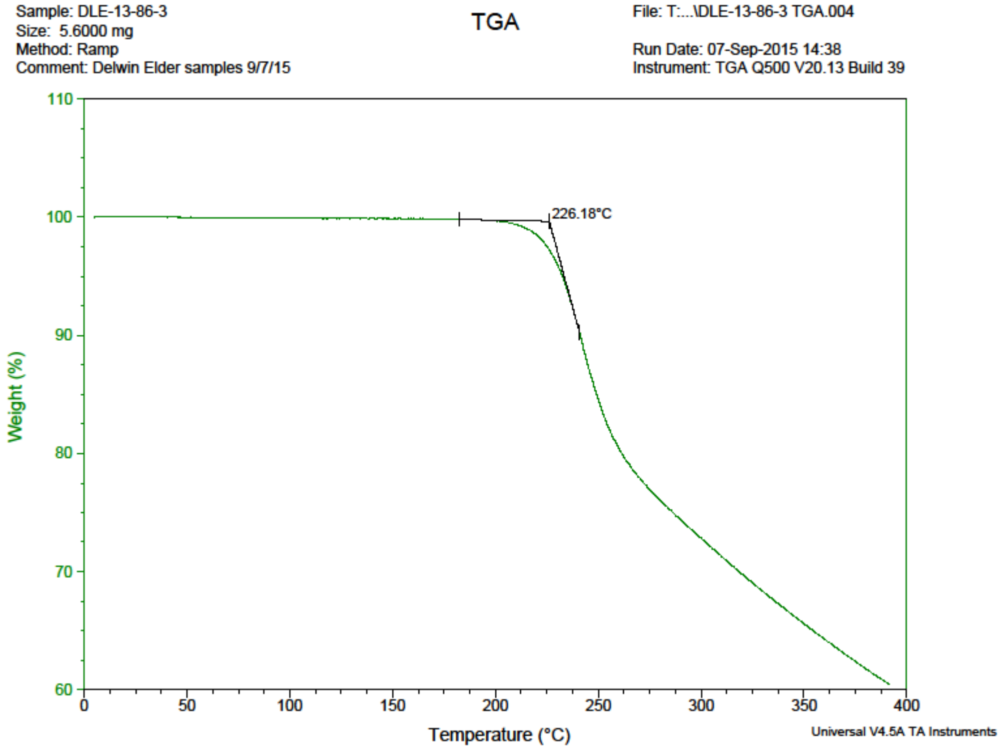

Figure S13. TGA plot of JRD1. T_d=226.18 °C.

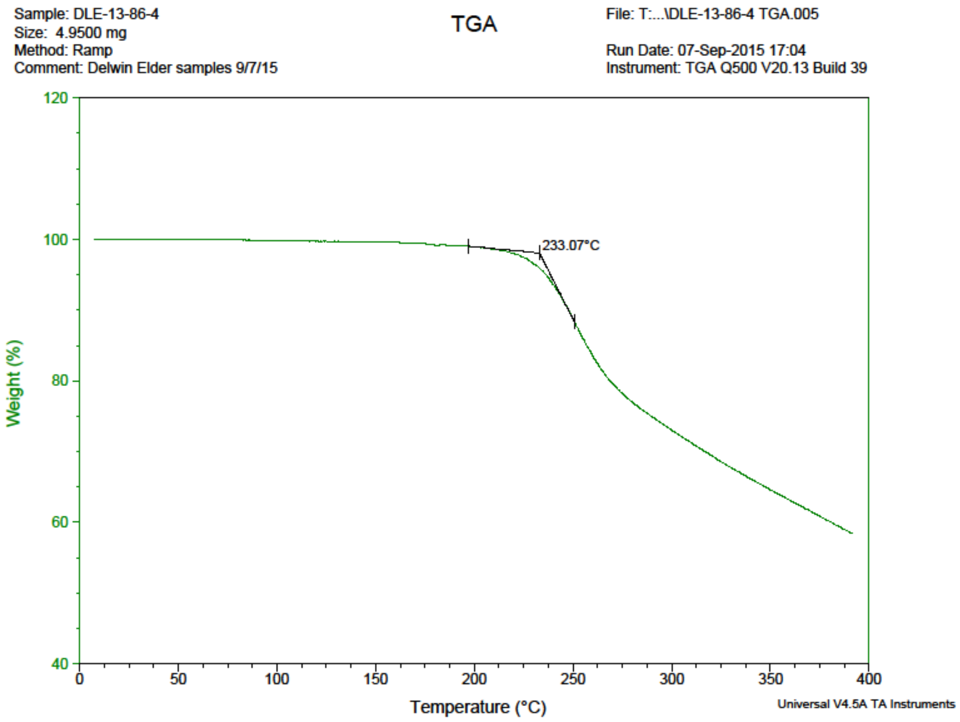

Figure S14. TGA plot of JRD5. T_d=233.07 °C.

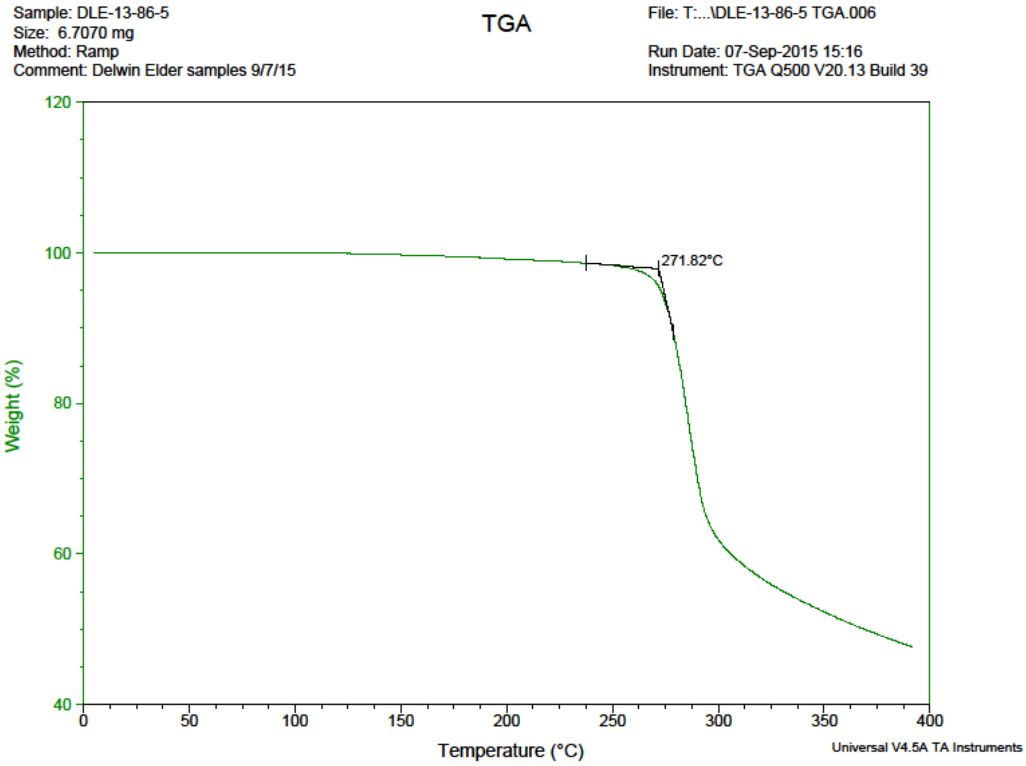

Figure S15. TGA plot of JRD2. T_d=271.82 °C.

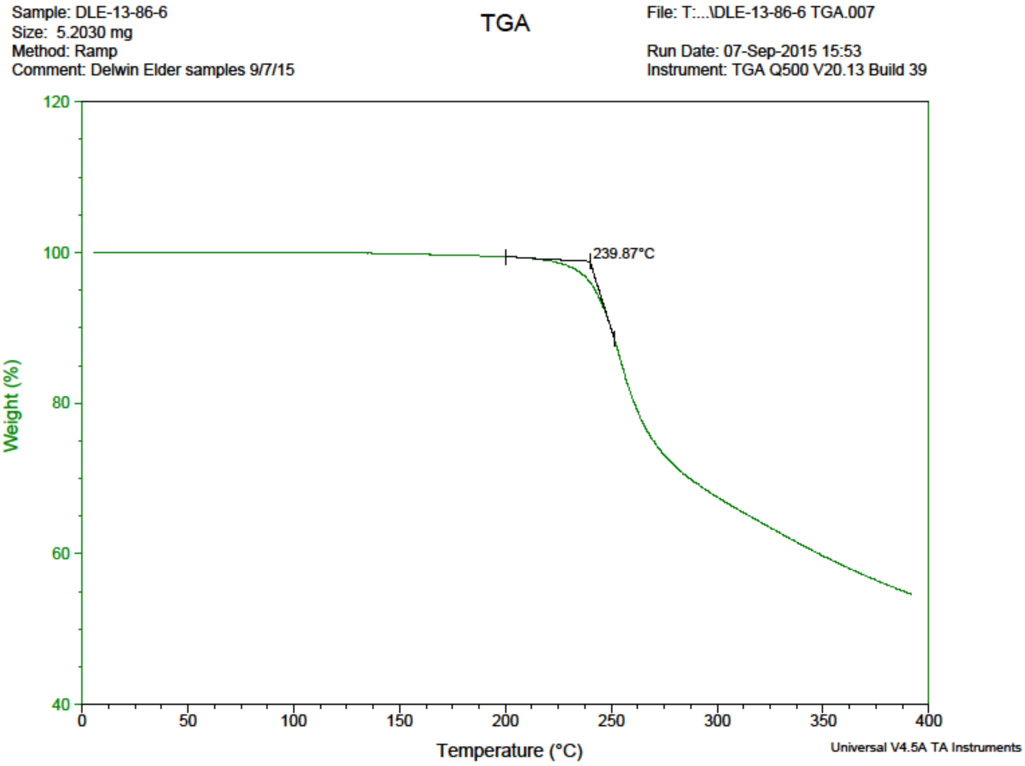

Figure S16. TGA plot of KRD1. T_d=239.87 °C.

Crystal Structure of YLD-124

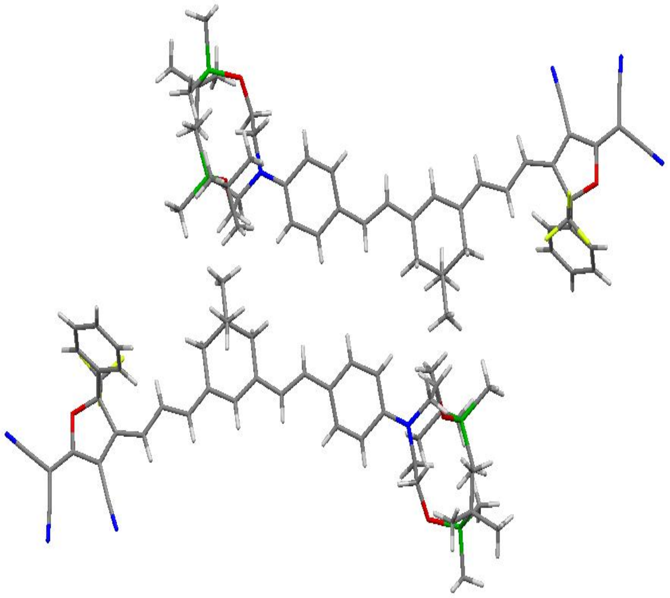

(a)

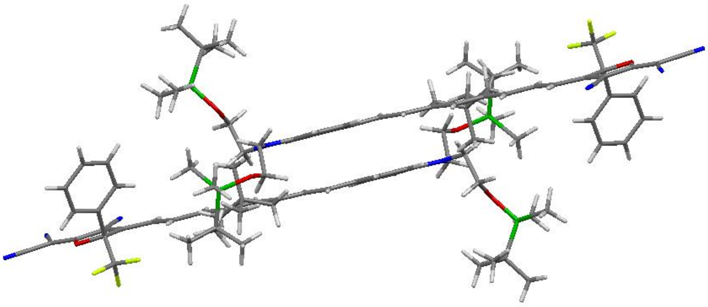

(b)

Figure S17. YLD-124 Crystal Structure, 2 molecules per unit cell, View (a) and (b).

Crystallization of YLD-124: Purified YLD-124 is dissolved in a minimal amount of DCM to form a concentrated ink. The ink is dropped into a scintillation vial which is then filled with cold methanol. The vial is fitted with a rubber septum and narrow gauge needle is placed in the septum such that the DCM can escape as it evaporates from the methanol solution. The vial is placed in a dark dry area. As the DCM evaporates, the molecules dimerize into a non-polar supermolecular structure that is insoluble in methanol and then further undergo polymerization. This process is competing with another process that degrades the chromophore.[30] A shiny, dark-copper colored, and delicate crystalline precipitate is formed over the course of several days. The degraded material is highly soluble in cold methanol and can be washed away without disturbing the crystalline material. The crystals are ribbon like and sub mm in size. The precipitate is filtered from the remaining methanol and washed with additional cold methanol.

The crystal structure data of YLD-124 was collected at -173 °C on a Bruker APEX II single crystal X-ray diffractometer, Mo-radiation. A lustrous, violet ultra-thin plate, measuring 0.30 x 0.15 x 0.01 mm^3 was mounted on a loop with oil. Crystal-to-detector distance was 40 mm and exposure time was 120 seconds per frame for all sets. The scan width was 1^{o}. Data collection was 97.1% complete to 25^{o} in ϑ. A total of 14385 reflections were collected covering the indices, h = -9 to 9, k = -16 to 16, l = -24 to 27. 8740 reflections were symmetry independent and the R_{int} = 0.1251 indicated that the data was of lesser than average quality (0.07). Indexing and unit cell refinement indicated a triclinic lattice. The space group was found to be P $\bar{1}$ (No.2).

The data was integrated and scaled using SAINT, SADABS within the APEX2 software package by Bruker.

Solution by direct methods (SHELXS, SIR97[11]) produced a complete heavy atom phasing model consistent with the proposed structure. The structure was completed by difference Fourier synthesis with SHELXL97.[31,32] Scattering factors are from Waasmair and Kirfel[33]. Hydrogen atoms were placed in geometrically idealised positions and constrained to ride on their parent atoms with C---H distances in the range 0.95-1.00 Angstrom. Isotropic thermal parameters U_{eq} were fixed such that they were $1.2U_{eq}$ of their parent atom U_{eq} for CH's and $1.5U_{eq}$ of their parent atom U_{eq} in case of methyl groups. All non-hydrogen atoms were refined anisotropically by full-matrix least-squares.

The structure is of high quality and ready for publication. Table S1 summarizes the data collection details. Atomic coordinates and equivalent isotropic displacement parameters are listed in Table S2. Information about bond lengths and angles could be found in Table S3. Figure S17 shows YLD-124 crystal structure.

Table S1. Crystallographic data for the structures provided.

Empirical formula	C50 H63 F3 N4 O3 Si2	
Formula weight	881.22	
Temperature	100(2) K	
Wavelength	0.71073 Å	
Crystal system	Triclinic	
Space group	P -1	
Unit cell dimensions	a = 7.905(7) Å	α = 105.216(17)°.
	b = 13.915(13) Å	β = 95.622(15)°.
	c = 22.51(2) Å	γ = 91.927(16)°.
Volume	2373(4) Å^3	
Z	2	
Density (calculated)	1.233 Mg/m^3	
Absorption coefficient	0.132 mm^{-1}	
F(000)	940	
Crystal size	0.30 x 0.15 x 0.01 mm^3	
Theta range for data collection	2.59 to 25.86°	
Index ranges	-9<=h<=9, -16<=k<=16, -24<=l<=27	
Reflections collected	14385	
Independent reflections	8740 [R(int) = 0.1251]	
Completeness to theta = 25.00°	97.1 %	
Max. and min. transmission	0.9987 and 0.9615	
Refinement method	Full-matrix least-squares on F^2	
Data / restraints / parameters	8740 / 66 / 573	
Goodness-of-fit on F^2	1.102	
Final R indices [I>2sigma(I)]	R1 = 0.1447, wR2 = 0.3453	
R indices (all data)	R1 = 0.2679, wR2 = 0.4199	
Extinction coefficient	0.025(5)	
Largest diff. peak and hole	0.591 and -0.439 e.Å^{-3}	

Table S2. Atomic coordinates (x 10^4) and equivalent isotropic displacement parameters (Å^2 x 10^3) for yld_124_0m. U(eq) is defined as one third of the trace of the orthogonalized U^{ij} tensor.

	x	y	z	U(eq)
C(1)	-5875(13)	13184(8)	6282(5)	35(3)
C(2)	-5120(12)	12569(7)	5793(5)	33(3)
C(3)	-4349(13)	11800(8)	5978(5)	36(3)
C(4)	-4527(13)	11972(7)	6670(5)	30(2)
C(5)	-2920(12)	12298(7)	7121(6)	35(3)
C(6)	-1324(13)	12109(8)	6929(6)	39(3)
C(7)	93(14)	12525(9)	7332(7)	49(3)
C(8)	-21(14)	13043(9)	7920(6)	43(3)
C(9)	-1617(16)	13258(9)	8102(6)	50(3)
C(10)	-3032(14)	12850(9)	7697(6)	43(3)
C(11)	-5607(15)	11143(8)	6805(5)	37(3)
C(12)	-6734(13)	14027(7)	6336(5)	36(3)
C(13)	-7308(14)	14516(8)	6924(6)	39(3)
C(14)	-7028(13)	14424(8)	5848(5)	32(2)
C(15)	-5137(12)	12712(8)	5196(6)	31(2)
C(16)	-3575(13)	11035(7)	5587(6)	37(3)
C(17)	-2765(13)	10230(7)	5713(6)	37(3)
C(18)	-2042(12)	9553(8)	5268(6)	42(3)
C(19)	-1218(13)	8737(8)	5343(5)	36(3)
C(20)	-1089(14)	8433(8)	5949(5)	42(3)
C(21)	530(13)	7845(7)	6028(5)	32(2)
C(22)	511(12)	6976(8)	5455(5)	32(2)
C(23)	274(12)	7254(8)	4858(5)	38(3)
C(24)	-553(13)	8095(7)	4836(6)	36(3)
C(25)	2117(13)	8523(9)	6136(6)	43(3)
C(26)	411(14)	7408(9)	6590(5)	41(3)
C(27)	808(12)	6667(7)	4312(5)	30(2)
C(28)	1689(12)	5821(7)	4281(5)	33(2)
C(29)	2303(12)	5230(7)	3747(5)	31(2)
C(30)	1947(13)	5301(8)	3148(5)	34(2)
C(31)	2523(15)	4710(9)	2657(6)	43(3)
C(32)	3609(14)	3902(8)	2730(6)	40(3)
C(33)	3945(13)	3795(8)	3324(5)	37(3)
C(34)	3302(13)	4434(7)	3828(6)	37(3)

C(35)	5256(15)	2508(8)	2299(6)	48(3)
C(36)	4130(20)	1591(10)	2309(6)	63(4)
C(37)	1980(18)	225(11)	542(7)	71(4)
C(38)	3650(20)	-803(10)	1451(7)	73(4)
C(39)	133(19)	-52(11)	1630(7)	64(4)
C(40)	-970(20)	802(14)	1563(9)	95(6)
C(41)	410(20)	-59(12)	2308(7)	81(5)
C(42)	-770(20)	-1014(14)	1231(8)	87(5)
C(43)	3771(15)	3373(9)	1627(6)	50(3)
C(44)	5000(20)	4105(12)	1441(7)	72(4)
C(45)	5390(30)	1984(15)	233(10)	118(7)
C(46)	5070(20)	3511(13)	-453(7)	84(5)
C(47)	8124(19)	3617(14)	464(8)	80(5)
C(48)	9050(30)	3164(16)	-90(10)	113(7)
C(49)	8820(50)	3320(30)	1008(15)	203(14)
C(50)	8470(40)	4710(20)	647(14)	167(10)
N(1)	-7714(13)	14878(8)	7378(6)	48(3)
N(2)	-7343(11)	14795(7)	5452(5)	43(2)
N(3)	-5146(10)	12761(7)	4708(5)	40(2)
N(4)	4157(12)	3302(7)	2236(5)	42(2)
O(1)	-5623(8)	12801(5)	6786(3)	37(2)
F(2)	-7007(7)	10912(5)	6407(3)	49(2)
F(1)	-6105(7)	11419(4)	7366(3)	44(2)
F(3)	-4765(7)	10335(4)	6781(3)	44(2)
O(2)	3129(14)	1262(7)	1735(5)	75(3)
O(3)	4736(13)	4026(7)	787(4)	68(3)
Si(1)	2217(5)	180(3)	1360(2)	58(1)
Si(2)	5882(6)	3310(3)	286(2)	66(1)

Table S3. Bond lengths [Å] and angles [°] for yld_124_0m.

C(1)-C(12)	1.360(14)
C(1)-O(1)	1.373(13)
C(1)-C(2)	1.404(15)
C(2)-C(3)	1.385(14)
C(2)-C(15)	1.407(16)
C(3)-C(16)	1.392(14)
C(3)-C(4)	1.535(15)
C(4)-O(1)	1.450(11)

C(4)-C(5)	1.521(15)
C(4)-C(11)	1.524(15)
C(5)-C(10)	1.334(16)
C(5)-C(6)	1.385(14)
C(6)-C(7)	1.376(16)
C(6)-H(6)	0.9500
C(7)-C(8)	1.344(17)
C(7)-H(7)	0.9500
C(8)-C(9)	1.383(17)
C(8)-H(8)	0.9500
C(9)-C(10)	1.375(17)
C(9)-H(9)	0.9500
C(10)-H(10)	0.9500
C(11)-F(3)	1.317(11)
C(11)-F(1)	1.323(13)
C(11)-F(2)	1.327(12)
C(12)-C(14)	1.357(16)
C(12)-C(13)	1.446(18)
C(13)-N(1)	1.097(14)
C(14)-N(2)	1.152(13)
C(15)-N(3)	1.119(13)
C(16)-C(17)	1.388(14)
C(16)-H(16)	0.9500
C(17)-C(18)	1.368(15)
C(17)-H(17)	0.9500
C(18)-C(19)	1.368(15)
C(18)-H(18)	0.9500
C(19)-C(24)	1.411(15)
C(19)-C(20)	1.526(16)
C(20)-C(21)	1.563(14)
C(20)-H(20A)	0.9900
C(20)-H(20B)	0.9900
C(21)-C(25)	1.504(15)
C(21)-C(22)	1.518(15)
C(21)-C(26)	1.550(15)
C(22)-C(23)	1.490(15)
C(22)-H(22A)	0.9900
C(22)-H(22B)	0.9900

C(23)-C(24)	1.369(14)
C(23)-C(27)	1.398(15)
C(24)-H(24)	0.9500
C(25)-H(25A)	0.9800
C(25)-H(25B)	0.9800
C(25)-H(25C)	0.9800
C(26)-H(26A)	0.9800
C(26)-H(26B)	0.9800
C(26)-H(26C)	0.9800
C(27)-C(28)	1.377(13)
C(27)-H(27)	0.9500
C(28)-C(29)	1.407(15)
C(28)-H(28)	0.9500
C(29)-C(30)	1.381(15)
C(29)-C(34)	1.422(14)
C(30)-C(31)	1.323(15)
C(30)-H(30)	0.9500
C(31)-C(32)	1.471(15)
C(31)-H(31)	0.9500
C(32)-N(4)	1.323(14)
C(32)-C(33)	1.386(16)
C(33)-C(34)	1.397(15)
C(33)-H(33)	0.9500
C(34)-H(34)	0.9500
C(35)-N(4)	1.455(13)
C(35)-C(36)	1.535(19)
C(35)-H(35A)	0.9900
C(35)-H(35B)	0.9900
C(36)-O(2)	1.403(15)
C(36)-H(36A)	0.9900
C(36)-H(36B)	0.9900
C(37)-Si(1)	1.851(16)
C(37)-H(37A)	0.9800
C(37)-H(37B)	0.9800
C(37)-H(37C)	0.9800
C(38)-Si(1)	1.844(14)
C(38)-H(38A)	0.9800
C(38)-H(38B)	0.9800

C(38)-H(38C)	0.9800
C(39)-C(42)	1.51(2)
C(39)-C(41)	1.52(2)
C(39)-C(40)	1.53(2)
C(39)-Si(1)	1.857(15)
C(40)-H(40A)	0.9800
C(40)-H(40B)	0.9800
C(40)-H(40C)	0.9800
C(41)-H(41A)	0.9800
C(41)-H(41B)	0.9800
C(41)-H(41C)	0.9800
C(42)-H(42A)	0.9800
C(42)-H(42B)	0.9800
C(42)-H(42C)	0.9800
C(43)-N(4)	1.405(16)
C(43)-C(44)	1.548(19)
C(43)-H(43A)	0.9900
C(43)-H(43B)	0.9900
C(44)-O(3)	1.443(17)
C(44)-H(44A)	0.9900
C(44)-H(44B)	0.9900
C(45)-Si(2)	1.84(2)
C(45)-H(45A)	0.9800
C(45)-H(45B)	0.9800
C(45)-H(45C)	0.9800
C(46)-Si(2)	1.817(18)
C(46)-H(46A)	0.9800
C(46)-H(46B)	0.9800
C(46)-H(46C)	0.9800
C(47)-C(49)	1.46(3)
C(47)-C(50)	1.47(3)
C(47)-C(48)	1.51(2)
C(47)-Si(2)	1.791(16)
C(48)-H(48A)	0.9800
C(48)-H(48B)	0.9800
C(48)-H(48C)	0.9800
C(49)-H(49A)	0.9801
C(49)-H(49B)	0.9801

C(49)-H(49C)	0.9801
C(50)-H(50A)	0.9800
C(50)-H(50B)	0.9800
C(50)-H(50C)	0.9800
O(2)-Si(1)	1.625(10)
O(3)-Si(2)	1.659(11)

C(12)-C(1)-O(1)	119.0(10)
C(12)-C(1)-C(2)	132.9(11)
O(1)-C(1)-C(2)	108.2(9)
C(3)-C(2)-C(1)	110.6(10)
C(3)-C(2)-C(15)	124.5(9)
C(1)-C(2)-C(15)	124.9(9)
C(2)-C(3)-C(16)	124.3(11)
C(2)-C(3)-C(4)	107.0(8)
C(16)-C(3)-C(4)	128.7(9)
O(1)-C(4)-C(5)	106.7(8)
O(1)-C(4)-C(11)	102.5(8)
C(5)-C(4)-C(11)	113.3(8)
O(1)-C(4)-C(3)	102.0(7)
C(5)-C(4)-C(3)	117.4(9)
C(11)-C(4)-C(3)	112.8(9)
C(10)-C(5)-C(6)	118.9(11)
C(10)-C(5)-C(4)	119.8(9)
C(6)-C(5)-C(4)	121.1(11)
C(7)-C(6)-C(5)	118.9(11)
C(7)-C(6)-H(6)	120.6
C(5)-C(6)-H(6)	120.6
C(8)-C(7)-C(6)	122.0(11)
C(8)-C(7)-H(7)	119.0
C(6)-C(7)-H(7)	119.0
C(7)-C(8)-C(9)	118.6(11)
C(7)-C(8)-H(8)	120.7
C(9)-C(8)-H(8)	120.7
C(10)-C(9)-C(8)	118.9(12)
C(10)-C(9)-H(9)	120.6
C(8)-C(9)-H(9)	120.6
C(5)-C(10)-C(9)	122.3(11)

C(5)-C(10)-H(10)	118.8
C(9)-C(10)-H(10)	118.8
F(3)-C(11)-F(1)	106.4(9)
F(3)-C(11)-F(2)	109.3(9)
F(1)-C(11)-F(2)	106.9(9)
F(3)-C(11)-C(4)	112.1(9)
F(1)-C(11)-C(4)	111.5(9)
F(2)-C(11)-C(4)	110.4(9)
C(14)-C(12)-C(1)	120.9(10)
C(14)-C(12)-C(13)	119.8(9)
C(1)-C(12)-C(13)	119.4(10)
N(1)-C(13)-C(12)	178.3(13)
N(2)-C(14)-C(12)	176.1(11)
N(3)-C(15)-C(2)	175.5(11)
C(17)-C(16)-C(3)	129.9(11)
C(17)-C(16)-H(16)	115.0
C(3)-C(16)-H(16)	115.0
C(18)-C(17)-C(16)	121.8(11)
C(18)-C(17)-H(17)	119.1
C(16)-C(17)-H(17)	119.1
C(19)-C(18)-C(17)	126.5(12)
C(19)-C(18)-H(18)	116.7
C(17)-C(18)-H(18)	116.7
C(18)-C(19)-C(24)	120.1(11)
C(18)-C(19)-C(20)	122.6(10)
C(24)-C(19)-C(20)	117.1(9)
C(19)-C(20)-C(21)	111.7(9)
C(19)-C(20)-H(20A)	109.3
C(21)-C(20)-H(20A)	109.3
C(19)-C(20)-H(20B)	109.3
C(21)-C(20)-H(20B)	109.3
H(20A)-C(20)-H(20B)	107.9
C(25)-C(21)-C(22)	112.3(9)
C(25)-C(21)-C(26)	109.7(9)
C(22)-C(21)-C(26)	107.7(8)
C(25)-C(21)-C(20)	110.5(9)
C(22)-C(21)-C(20)	108.0(9)
C(26)-C(21)-C(20)	108.5(9)

C(23)-C(22)-C(21)	114.6(9)
C(23)-C(22)-H(22A)	108.6
C(21)-C(22)-H(22A)	108.6
C(23)-C(22)-H(22B)	108.6
C(21)-C(22)-H(22B)	108.6
H(22A)-C(22)-H(22B)	107.6
C(24)-C(23)-C(27)	118.6(11)
C(24)-C(23)-C(22)	119.0(10)
C(27)-C(23)-C(22)	122.4(10)
C(23)-C(24)-C(19)	124.9(11)
C(23)-C(24)-H(24)	117.6
C(19)-C(24)-H(24)	117.6
C(21)-C(25)-H(25A)	109.5
C(21)-C(25)-H(25B)	109.5
H(25A)-C(25)-H(25B)	109.5
C(21)-C(25)-H(25C)	109.5
H(25A)-C(25)-H(25C)	109.5
H(25B)-C(25)-H(25C)	109.5
C(21)-C(26)-H(26A)	109.5
C(21)-C(26)-H(26B)	109.5
H(26A)-C(26)-H(26B)	109.5
C(21)-C(26)-H(26C)	109.5
H(26A)-C(26)-H(26C)	109.5
H(26B)-C(26)-H(26C)	109.5
C(28)-C(27)-C(23)	123.7(10)
C(28)-C(27)-H(27)	118.1
C(23)-C(27)-H(27)	118.1
C(27)-C(28)-C(29)	125.6(11)
C(27)-C(28)-H(28)	117.2
C(29)-C(28)-H(28)	117.2
C(30)-C(29)-C(28)	126.8(9)
C(30)-C(29)-C(34)	116.7(10)
C(28)-C(29)-C(34)	116.4(10)
C(31)-C(30)-C(29)	124.6(10)
C(31)-C(30)-H(30)	117.7
C(29)-C(30)-H(30)	117.7
C(30)-C(31)-C(32)	119.9(11)
C(30)-C(31)-H(31)	120.0

C(32)-C(31)-H(31)	120.0
N(4)-C(32)-C(33)	123.6(10)
N(4)-C(32)-C(31)	119.7(11)
C(33)-C(32)-C(31)	116.7(10)
C(32)-C(33)-C(34)	121.4(10)
C(32)-C(33)-H(33)	119.3
C(34)-C(33)-H(33)	119.3
C(33)-C(34)-C(29)	120.6(11)
C(33)-C(34)-H(34)	119.7
C(29)-C(34)-H(34)	119.7
N(4)-C(35)-C(36)	108.5(10)
N(4)-C(35)-H(35A)	110.0
C(36)-C(35)-H(35A)	110.0
N(4)-C(35)-H(35B)	110.0
C(36)-C(35)-H(35B)	110.0
H(35A)-C(35)-H(35B)	108.4
O(2)-C(36)-C(35)	108.2(11)
O(2)-C(36)-H(36A)	110.1
C(35)-C(36)-H(36A)	110.1
O(2)-C(36)-H(36B)	110.1
C(35)-C(36)-H(36B)	110.1
H(36A)-C(36)-H(36B)	108.4
Si(1)-C(37)-H(37A)	109.5
Si(1)-C(37)-H(37B)	109.5
H(37A)-C(37)-H(37B)	109.5
Si(1)-C(37)-H(37C)	109.5
H(37A)-C(37)-H(37C)	109.5
H(37B)-C(37)-H(37C)	109.5
Si(1)-C(38)-H(38A)	109.5
Si(1)-C(38)-H(38B)	109.5
H(38A)-C(38)-H(38B)	109.5
Si(1)-C(38)-H(38C)	109.5
H(38A)-C(38)-H(38C)	109.5
H(38B)-C(38)-H(38C)	109.5
C(42)-C(39)-C(41)	111.5(14)
C(42)-C(39)-C(40)	107.6(15)
C(41)-C(39)-C(40)	109.7(12)
C(42)-C(39)-Si(1)	111.3(10)

C(41)-C(39)-Si(1)	109.2(11)
C(40)-C(39)-Si(1)	107.3(11)
C(39)-C(40)-H(40A)	109.5
C(39)-C(40)-H(40B)	109.5
H(40A)-C(40)-H(40B)	109.5
C(39)-C(40)-H(40C)	109.5
H(40A)-C(40)-H(40C)	109.5
H(40B)-C(40)-H(40C)	109.5
C(39)-C(41)-H(41A)	109.5
C(39)-C(41)-H(41B)	109.5
H(41A)-C(41)-H(41B)	109.5
C(39)-C(41)-H(41C)	109.5
H(41A)-C(41)-H(41C)	109.5
H(41B)-C(41)-H(41C)	109.5
C(39)-C(42)-H(42A)	109.5
C(39)-C(42)-H(42B)	109.5
H(42A)-C(42)-H(42B)	109.5
C(39)-C(42)-H(42C)	109.5
H(42A)-C(42)-H(42C)	109.5
H(42B)-C(42)-H(42C)	109.5
N(4)-C(43)-C(44)	113.8(10)
N(4)-C(43)-H(43A)	108.8
C(44)-C(43)-H(43A)	108.8
N(4)-C(43)-H(43B)	108.8
C(44)-C(43)-H(43B)	108.8
H(43A)-C(43)-H(43B)	107.7
O(3)-C(44)-C(43)	111.6(11)
O(3)-C(44)-H(44A)	109.3
C(43)-C(44)-H(44A)	109.3
O(3)-C(44)-H(44B)	109.3
C(43)-C(44)-H(44B)	109.3
H(44A)-C(44)-H(44B)	108.0
Si(2)-C(45)-H(45A)	109.5
Si(2)-C(45)-H(45B)	109.5
H(45A)-C(45)-H(45B)	109.5
Si(2)-C(45)-H(45C)	109.5
H(45A)-C(45)-H(45C)	109.5
H(45B)-C(45)-H(45C)	109.5

Si(2)-C(46)-H(46A)	109.5
Si(2)-C(46)-H(46B)	109.5
H(46A)-C(46)-H(46B)	109.5
Si(2)-C(46)-H(46C)	109.5
H(46A)-C(46)-H(46C)	109.5
H(46B)-C(46)-H(46C)	109.5
C(49)-C(47)-C(50)	103(2)
C(49)-C(47)-C(48)	111(2)
C(50)-C(47)-C(48)	109.1(19)
C(49)-C(47)-Si(2)	112.0(19)
C(50)-C(47)-Si(2)	110.3(15)
C(48)-C(47)-Si(2)	110.6(12)
C(47)-C(48)-H(48A)	109.5
C(47)-C(48)-H(48B)	109.5
H(48A)-C(48)-H(48B)	109.5
C(47)-C(48)-H(48C)	109.5
H(48A)-C(48)-H(48C)	109.5
H(48B)-C(48)-H(48C)	109.5
C(47)-C(49)-H(49A)	109.3
C(47)-C(49)-H(49B)	109.5
H(49A)-C(49)-H(49B)	109.5
C(47)-C(49)-H(49C)	109.7
H(49A)-C(49)-H(49C)	109.5
H(49B)-C(49)-H(49C)	109.5
C(47)-C(50)-H(50A)	109.5
C(47)-C(50)-H(50B)	109.5
H(50A)-C(50)-H(50B)	109.5
C(47)-C(50)-H(50C)	109.4
H(50A)-C(50)-H(50C)	109.5
H(50B)-C(50)-H(50C)	109.5
C(32)-N(4)-C(43)	124.4(10)
C(32)-N(4)-C(35)	120.6(11)
C(43)-N(4)-C(35)	115.0(9)
C(1)-O(1)-C(4)	111.6(8)
C(36)-O(2)-Si(1)	132.2(8)
C(44)-O(3)-Si(2)	121.9(9)
O(2)-Si(1)-C(38)	109.1(6)
O(2)-Si(1)-C(37)	104.0(6)

C(38)-Si(1)-C(37)	109.6(7)
O(2)-Si(1)-C(39)	112.3(6)
C(38)-Si(1)-C(39)	109.8(7)
C(37)-Si(1)-C(39)	111.9(7)
O(3)-Si(2)-C(47)	113.1(6)
O(3)-Si(2)-C(46)	103.6(7)
C(47)-Si(2)-C(46)	112.1(9)
O(3)-Si(2)-C(45)	110.2(7)
C(47)-Si(2)-C(45)	110.7(10)
C(46)-Si(2)-C(45)	106.8(9)

Theory

Donor Study:

All calculations were performed with the Gaussian-09 Rev D.01 electronic structure package (Frisch 2013)[34]. The molecular geometries were optimized in vacuum at the B3LYP/6-31+G* level of theory using an "ultrafine" integration grid and tightened convergence settings (i.e., "Opt=Tight"), which choose the RMS force on all atoms to converge at a threshold of 1 x 10^{-5} au or less. All calculations were carried out according to default SCF convergence criteria, requiring density matrix convergence at least 10^{-8} au.

Dipole moments and static and frequency-dependent (hyper)polarizabilities were computed with a long-range corrected (LC) functional, LC-BLYP (Iikura 2001)[35]. Static hyperpolarizability, $\beta_{zzz}(0)$, and Pockels hyperpolarizability consistent with measurements of poling efficiency, $\beta_{zzz}(-\omega;\omega,0)$, at 1310-nm were computed via analytic differentiation by the coupled-perturbed Kohn-Sham (CPKS) method (Kamiya 2005)[36]. Changes in computed electronic and optical properties as a result of changing dielectric environment were also studied using the polarizable continuum model (PCM). See Tables S4-S6.

Excitation energies were computed with B3LYP with 6-31+G* basis set using the linear response time-dependent DFT formalism in solvent media (chloroform and acetonitrile) with PCM.

Table S4. Dipole moments, polarizabilities, and hyperpolarizabilities calculated using LC-BLYP/6-31+G* **in Vacuo**; given according to the perturbation convention. Frequency-dependent properties are computed at 1310-nm.

Structures	μ_z (D)	$\alpha_{zz}(-\omega;\omega)$ x10^{-24} esu	$\beta_{zzz}(0)$ x10^{-30} esu	$\beta_{zzz}(-\omega;\omega,0)$ x10^{-30} esu
JRD1	21.4	308	483	680
YLD124	22.0	171	460	641
AJY1	22.6	248	444	623
JRD2	17.6	151	87.9	108
KRD1	20.0	190	341	463
JRD5	20.3	304	476	664

Table S5. Dipole Moments, polarizabilities, hyperpolarizabilities, and wavelength of maximum absorption (λ_{max}) calculated using LC-BLYP/6-31+G* **in Chloroform**; given according to the perturbation convention. Frequency-dependent properties are computed at 1310-nm.

Structures	μ_z (D)	$\alpha_{zz}(-\omega;\omega)$ x10^{-24} esu	$\beta_{zzz}(0)$ x10^{-30} esu	$\beta_{zzz}(-\omega;\omega,0)$ x10^{-30} esu	λ_{max} (nm)
JRD1	26.1	398	1245	1567	731.01
YLD124	27.1	210	1231	1536	729.74
AJY1	28.3	342	1334	1659	738.14

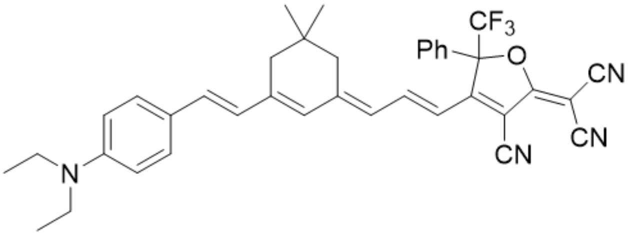

AJY1

Table S6. Dipole moments, polarizabilities, hyperpolarizabilities, and wavelength of maximum absorption (λ_{max}) calculated using LC-BLYP/6-31+G* **in Acetonitrile**; given according to the perturbation convention. Frequency-dependent properties are computed at 1310-nm.

Structures	μ_z (D)	$\alpha_{zz}(-\omega;\omega)$ x10^{-24} esu	$\beta_{zzz}(0)$ x10^{-30} esu	$\beta_{zzz}(-\omega;\omega,0)$ x10^{-30} esu	λ_{max} (nm)
JRD1	27.7	398.7	1768	1695*	729.09
YLD124	29.0	209	1782	1695*	729.71
AJY1	30.3	343	1980	1840*	737.99

*Note that $\beta_{zzz}(-\omega;\omega,0) < \beta_{zzz}(0)$; this commonly occurs with highly polar solvents.

In the HOMO-LUMO structures, you can see that the TBDPS and TBDMS groups do not participate greatly in the electronic structures. The HOMO-LUMO structures are similar for the series, based both on MO visualization and energy levels. Below in Figures S18-S20 are the HOMO and LUMO structures according to B3LYP/6-31+G* and wB97xD/6-31+G*. The HOMO structures are qualitatively similar across the DFT methods; however, LUMO for wB97xD is much less localized on the donor phenyl ring than shown in B3LYP. Nevertheless, the LUMO structures are similar for AJY1, JRD1, and YLD124 within a given DFT method (wB97xD or B3LYP).

B3LYP	**wB97xD**
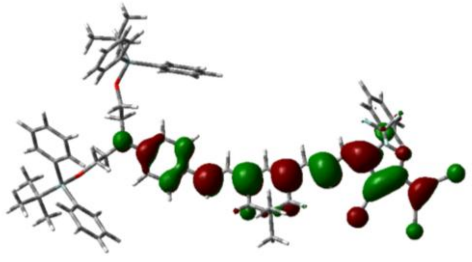 **LUMO**	**LUMO** 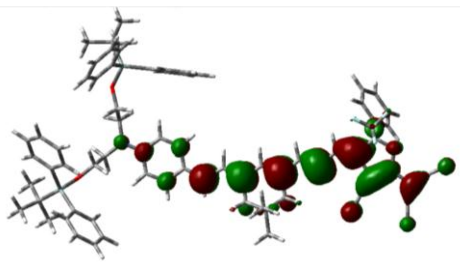
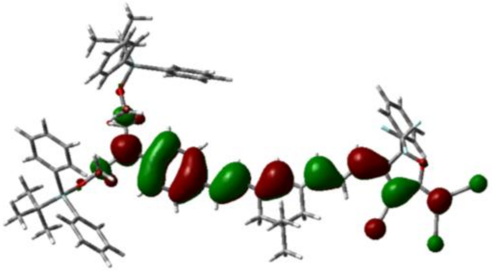 **HOMO**	**HOMO** 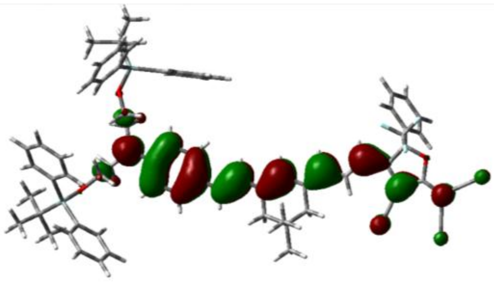

Figure S18. JRD1 Molecular Orbital structures DFT/6-31+G*//B3LYP/6-31+G* in Chloroform (PCM)

B3LYP	**wB97xD**

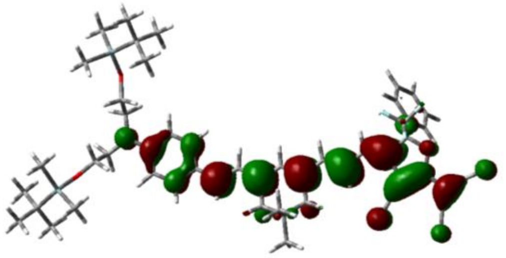 **LUMO**	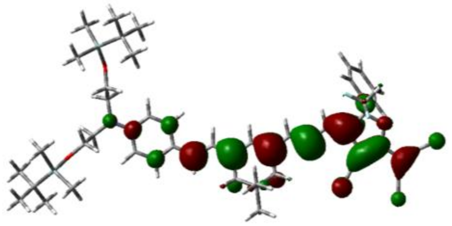 **LUMO**
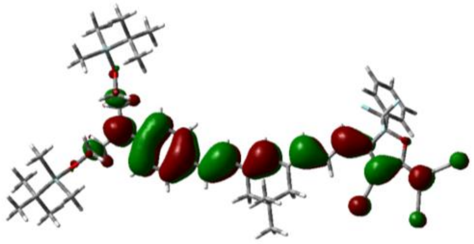 **HOMO**	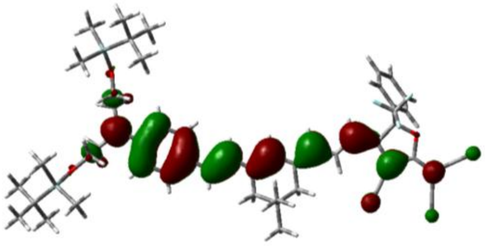 **HOMO**

Figure S19. YLD124 Molecular Orbital structures DFT/6-31+G*//B3LYP/6-31+G* in Chloroform (PCM)

B3LYP	**wB97xD**
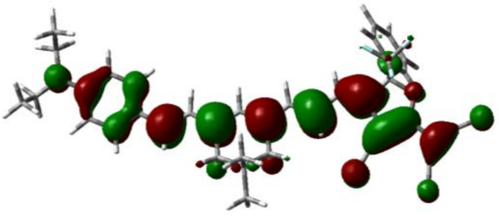 **LUMO**	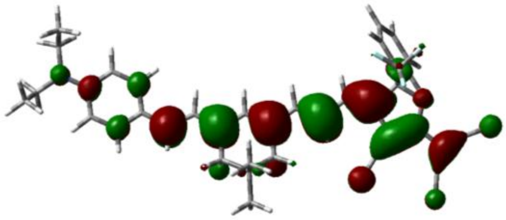 **LUMO**
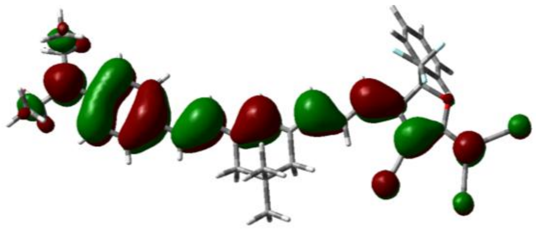 **HOMO**	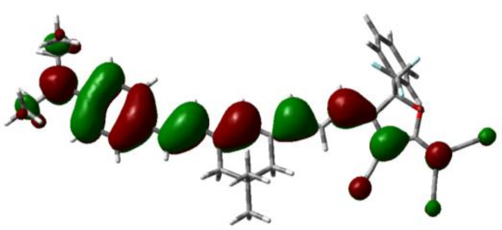 **HOMO**

Figure S20. AJY1 Molecular Orbital structures DFT/6-31+G*//B3LYP/6-31+G* in Chloroform (PCM)

JRD5	**JRD1**

LUMO 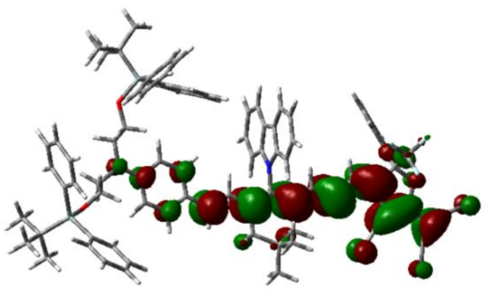 **ε_{LUMO} = -2.2773 eV** **HOMO** 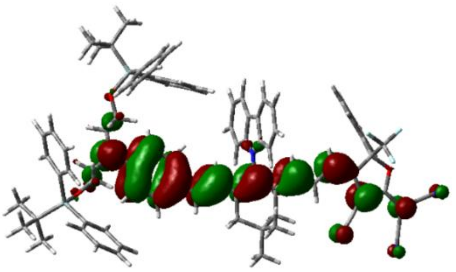 **ε_{HOMO} = -6.9841 eV**	**LUMO** 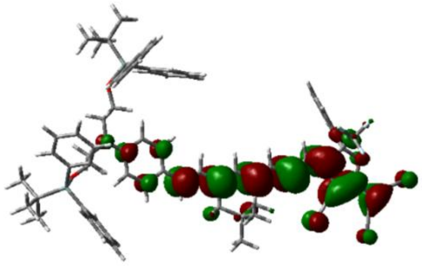 **ε_{LUMO} = -2.2351 eV** **HOMO** 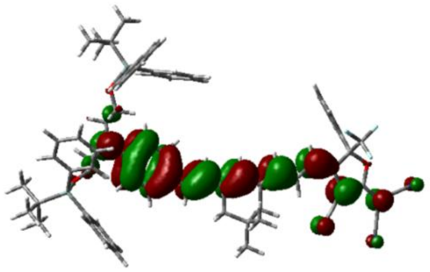 **ε_{HOMO} = -6.9046 eV** (Approx. 0.08 eV higher than JRD5 ε_{HOMO})

Figure S21. Side-by-side comparison of JRD5 and JRD1 molecular orbital structures according to wB97xD with 6-31+G* basis set and B3LYP/6-31+G* optimized geometry in Chloroform (PCM)

The frontier molecular orbitals of JRD1 and JRD5 are shown in Figure S21, according to wB97D/6-31+G*//B3LYP/6-31+G* in chloroform (PCM). The highest occupied molecular orbitals (HOMO) of the two species are generally similar and are delocalized over the length of the π-conjugated bridge, however the visualization shows that the carbazole in JRD5 offers a small electron-donating contribution. The lowest unoccupied molecular orbitals (LUMO) are similar for both structures and have only approximately 0.04 eV energy difference between JRD1 and JRD5. It follows that the intramolecular charge transfer transition energies ($\Delta E_{HOMO-LUMO}$) from HOMO-LUMO are similar between JRD1 and JRD5 with approximately 0.04 eV difference. It is important to note that the HOMO-LUMO energy difference, $\Delta E_{HOMO-LUMO}$, is not equal to the peak vertical excitation energy (i.e., λ_{max}) which involves a mixing of contributions from various excited states.

The frontier molecular orbitals of JRD1 and JRD5 according to B3LYP/6-31+G*//B3LYP/6-31+G* in chloroform (PCM) are shown in Figure S22. Similar to the long-range corrected method results (wB97xD; Figure S21), the HOMO visualization shows that the carbazole in JRD5 offers a small electron-donating contribution. The HOMO and LUMO energy values of JRD1 are shifted approx. 0.07 eV higher than those of JRD5. Consequently, the intramolecular charge transfer transition energies ($\Delta E_{HOMO-LUMO}$) from HOMO-LUMO are practically identical.

JRD5	**JRD1**
LUMO	**LUMO**
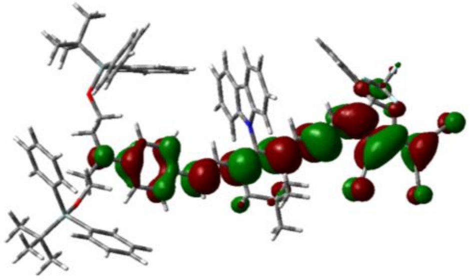	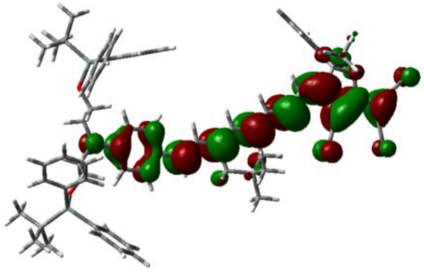
$\varepsilon_{\mathrm{LUMO}} = -3.5944$ eV	**$\varepsilon_{\mathrm{LUMO}} = -3.5353$ eV**
HOMO	**HOMO**
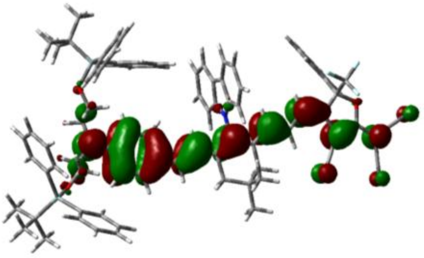	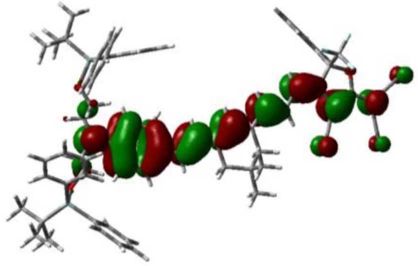
$\varepsilon_{\mathrm{HOMO}} = -5.4292$ eV	**$\varepsilon_{\mathrm{HOMO}} = -5.3560$ eV** (Approx. 0.07 eV higher than JRD5 $\varepsilon_{\mathrm{HOMO}}$)

Figure S22. Side-by-side comparison of JRD5 and JRD1 molecular orbital structures according to B3LYP with 6-31+G* basis set and B3LYP/6-31+G* optimized geometry in Chloroform (PCM)

B3LYP	**wB97xD**
LUMO	**LUMO**
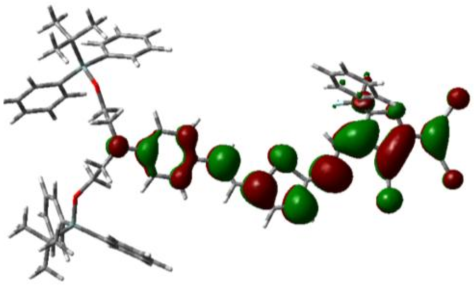	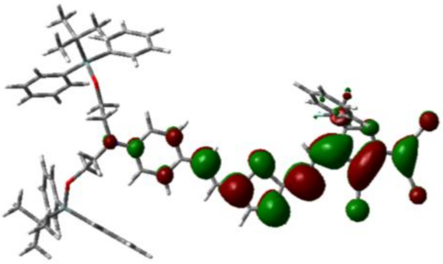
$\varepsilon_{\mathrm{LUMO}} = -3.6031$ eV	**$\varepsilon_{\mathrm{LUMO}} = -2.2553$ eV**
HOMO	**HOMO**
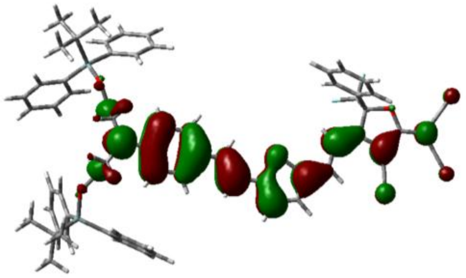	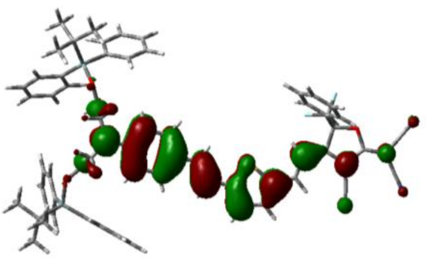
$\varepsilon_{\mathrm{HOMO}} = -5.4298$ eV	**$\varepsilon_{\mathrm{HOMO}} = -7.0077$ eV**

Figure S23. Side-by-side comparison of B3LYP and wB97xD results for molecule KRD1: Molecular Orbital structures

The frontier molecular orbitals of KRD1 according to different DFT methods: B3LYP and wB97xD, both with 6-31+G* basis set and B3LYP optimized geometry in chloroform (PCM) are shown in Figure S23. As expected with the inclusion of long-range (LR) Hartree Fock (HF) exchange in wB97xD, the predicted intramolecular charge transfer transition energy ($\Delta E_{HOMO\text{-}LUMO}$) from HOMO-LUMO is significantly larger (blue-shifted) in comparison to B3LYP which has no LR HF exchange correction. Within a given DFT method, the energy results for KRD1 are similar to JRD1 and JRD5.

The frontier molecular orbitals of JRD2 according to different DFT methods: B3LYP and wB97xD, both with 6-31+G* basis set and B3LYP optimized geometry in chloroform (PCM) are shown in Figure S24. The smaller bridge structure results in an overall larger energy CT transition (blue shift) than predicted for JRD1, JRD5, or KRD1.

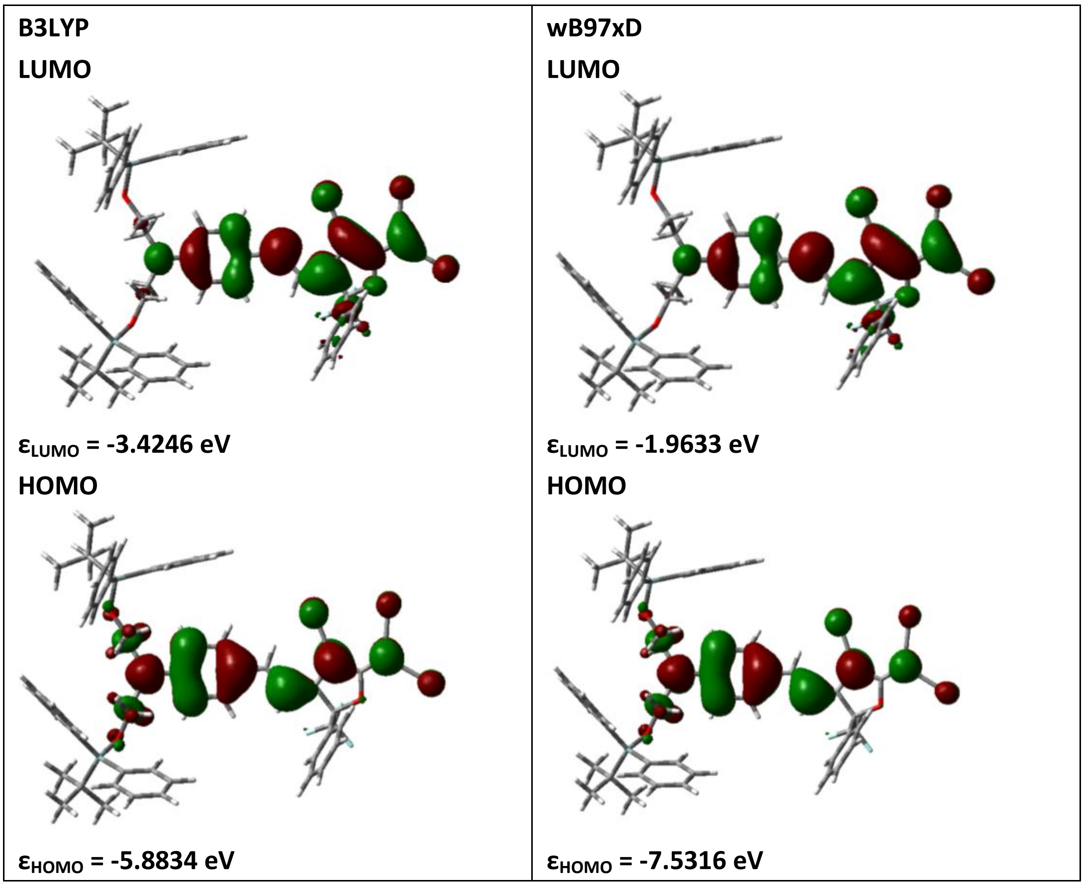

Figure S24. Side-by-side comparison of B3LYP and wB97xD results for molecule JRD2: Molecular Orbital structures

Device Fabrication

ITO/glass substrates were scrubbed with a cotton swab and multi-purpose detergent. Then slides were rinsed with deionized water, and fixed vertically on a polyethylene block where they were first immersed in acetone and sonicated for 5-10 minutes followed by immersion in isopropanol and another sonication for 5-10 minutes.

Solutions of 9-12% w/w EO material in TCE were filtered through a 0.2 μm PTFE filter and spin cast on ITO/Glass substrates to form neat thin films. EO films were spin cast in three stages, 500 rpm for 5 seconds, 850 rpm for 30 seconds, followed immediately by 2000 rpm for 30 seconds. The films were then dried on a hot plate at 65 ˚C for half an hour, and then further cured in a vacuum oven at 65 ˚C overnight. The thickness of the EO film was then measured to be around 1-2 μm via optical profilometry. Gold electrodes (~60 nm thick) were deposited on top of the films by sputter coating.

Results and Discussion:

Device conductance

High device conductance caused by chromophore conductivity at elevated temperature during poling limits the EO activity and needs to be controlled. There have been previous efforts to control this by introducing barrier layers,[37,38] but certain barrier layers (e.g. solvent cast) are not easy to apply to device structures with vertical electrode walls, such as silicon slot waveguides used in SOH modulators. We found in our research that molecular modification might help to reduce poling-induced conductance in high ρ_N chromophores.

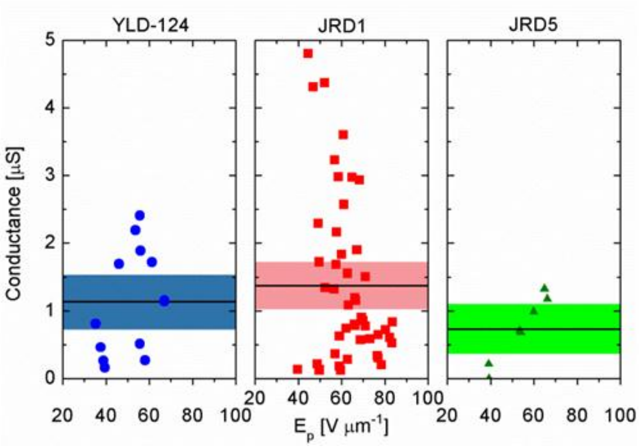

Figure S25. The average conductance (G) during the poling process of JRD1-based devices (red square, G = 1.37 ± 0.35 μS), YLD-124-based devices (blue dot, G = 1.13 ± 0.40 μS), and JRD5-based devices (green triangle, G = 0.73 ± 0.36 μS). Red, green, and blue bands represent the 95% confidence intervals of the mean conductance.

The conductance of YLD-124, JRD1 and JRD5 devices were calculated from the measured current and voltage as a function of the average poling field during the poling process (Figure S25). JRD5 devices showed relative low conductance, while JRD1 and YLD-124 devices had similarly high conductance behavior. This figure indicates that the conductivity of monolithic materials can be affected by tuning of the bulk electronic mobility through bridge modification. This could be a noteworthy area for future study to solve the high conductivity problem of high number-density materials, in addition to the current barrier layer solution.

Additional information for poling results:

Table S7. Average electric field during poling for the max r_{33}

EO material	Barrier layer	Electric field E_p /(V µm^{-1})	Max r_{33} /(pm V^{-1})	r_{33}/E_p /(nm/V)^2
YLD-124	With BCB	75	242	3.2
	No barrier	57	118	2.1
JRD1	With BCB	85	556	6.5
	No barrier	77	343	4.5
JRD5	With BCB	75	214	2.9
	No barrier	65	188	2.9
JRD2	No barrier	54	22	0.4
KRD1	No barrier	110	155	1.4

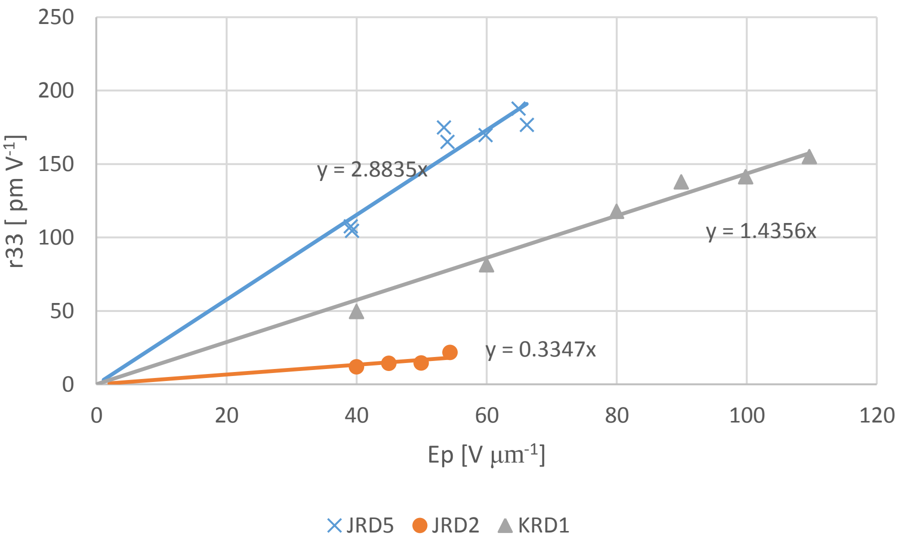

Figure S26. Poling curves for JRD5, JRD2 and KRD1.

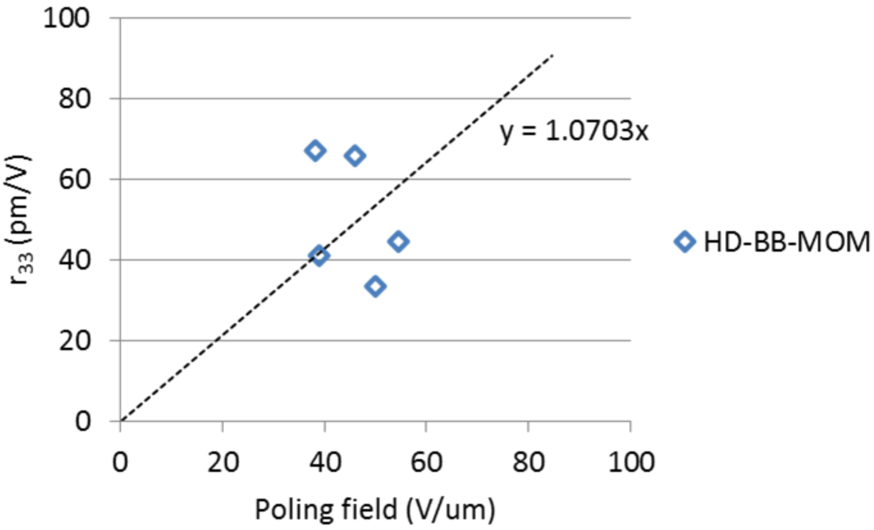

Figure S27. r_{33} vs. poling field plot for HD-BB-MOM.

For more detailed information about statistical analysis, analysis of average electric field strength during poling, and the calculation of the device conductance, please see reference 37 and its supporting information.

REFERENCE

1. B. Olbricht, Ph.D. Thesis, University of Washington, 2010.
2. S. Li. Reverse synthetic methods for making organic non-linear optical materials, December 29 2005. US Patent App. 10/876,322.
3. C. Zhang, L. R. Dalton, M.-C. Oh, H. Zhang, and W. H. Steier, *Chem. Mater.*, 2001, **13**, 3043-3050.
4. J. Luo, Y. Cheng, T.-D. Kim, S. Hau, S.-H. Jang, Z. Shi, X.-H. Zhou, and A. K.-Y. Jen, *Org. Lett.*, 2006, **8**, 1387-1390.
5. C. G. Overberger, J. C. Salamone, J. Ebenda, *Organic chemistry of synthetic high polymers.* robert w. lenz. interscience (wiley), new york, 1967. xvi + 837 pp., illus. Science, 159(3820):1224, 1968.
6. orgsyn.org. Organic synthesis, 2015.
7. M. C. Davis, R. A. Hollins, and B. Douglas, *Synth. Commun.*, 2006, **36**, 3515-3523.
8. S. Guang, S. Yin, H. Xu, W. Zhu, Y. Gao, and Y. Song, *Dyes and pigments*, 2007, **73**, 285-291.
9. I. V. Kosilkin, Ph.D. Thesis, University of Washington, 2012.
10. T. Baehr-Jones, M. Hochberg, G. Wang, R. Lawson, Y. Liao, P. Sullivan, L. Dalton, A. K.-Y. Jen, and A. Scherer, *Opt. Express*, 2005, **13**, 5216-5226.
11. E. Knoevenagel, *Berichte der deutschen chemischen Gesellschaft*, 1898, **31**, 2596-2619.
12. W. C. Still, M. Kahn, and A. Mitra, *J. Org. Chem.*, 1978, **43**, 2923-2925.
13. E. J. Corey and A. Venkateswarlu, *J. Am. Chem. Soc.*, 1972, **94**, 6190-6191.
14. I. V. Kosilkin, E. A. Hillenbrand, P. Tongwa, A. Fonari, J. Zazueta, M. S. Fonari, M. Antipin, L. R. Dalton, and T. Timofeeva, *Journal of Molecular Structure*, 2011, **1006**, 356-365.
15. Peter G. M. Wuts and Theodora W. Greene. Greene's Protective Groups in Organic Synthesis. Wiley Online Library: Books. Wiley, 2006.
16. D. L. Elder, S. J. Benight, J. Song, B. H. Robinson and L. R. Dalton, *Chem. Mater.*, 2014, **26**, 872-874.
17. W. S. Wadsworth. *Synthetic Applications of Phosphoryl-Stabilized Anions*. John Wiley & Sons, Inc., 2004.
18. W. S. Wadsworth and W. D. Emmons, *J. Am. Chem. Soc.*, 1961, **83**, 1733-1738.

19. J. Luo, S. Huang, Y. J. Cheng, T. D. Kim, Z. Shi, X. H. Zhou, and A. K.-Y. Jen, *Org. lett.*, 2007, **9**, 4471-4474.
20. M. He, T. M. Leslie, and J. A. Sinicropi. *Chem. Mater.*, 2002, **14**, 2393-2400.
21. G. Melikian, F. P. Rouessac, and C. Alexandre, *Synth. Commun.*, 1995, **25**, 3045-3051.
22. M. M. Mojtahedi, M. S. Abaee, M. M. Zahedi, M. R. Jalali, A. W. Mesbah, W. Massa, R. Yaghoubi, and M. Forouzani, *Monatshefte für Chemie-Chemical Monthly*, 2008, **139**, 917-921.
23. H. Meislich and S. Jasne, *J. Org. Chem.*, 1975, **40**, 2662-2666.
24. B. Rissafi, N. Rachiqi, A. El Louzi, A. Loupy, A. Petit, and S. Fkih-Ttouani, *Tetrahedron*, 2001, **57**, 2761 -2768.
25. L. R. Dalton, P. A. Sullivan, and D. H. Bale, *Chem. Rev.*, 2010, **110**, 25-55.
26. J. A. Davies, A. Elangovan, P. A. Sullivan, B. C. Olbricht, D. H. Bale, T. R. Ewy, C. M. Isborn, B. E. Eichinger, B. H. Robinson, P. J. Reid, X. Li and L. R. Dalton, *J. Am. Chem. Soc.*, 2008, **130**, 10565-10575.
27. T.-D. Kim, J.-W. Kang, J. Luo, S.-H. Jang, J.-W. Ka, N. Tucker, J. B. Benedict, L. R. Dalton, T. Gray, R. M. Overney, D. H. Park, W. N. Herman and A. K. -Y. Jen, *J. Am. Chem. Soc.*, 2007, **129**, 488-489.
28. S. J. Benight, Ph.D. Thesis, University of Washington, 2011.
29. D. L. Elder, S. J. Benight, J. Song, B. H. Robinson and L. R. Dalton, *Chem. Mater.*, 2014, **26**, 872 – 874.
30. A. Altomare, C. Burla, M. Camalli, G. L. Cascarano, C. Giacovazzo, A. Guagliardi, A. G. Moliterni, G. Polidori, and R. Spagna, *Journal of Applied Crystallography*, 1999, **32**, 115-119; A. Altomare, G. L. Cascarano, C. Giacovazzo, and A. Guagliardi, *Journal of Applied Crystallography*, 1993, **26**, 343-350.
31. Sheldrick GM. SHELXL-97, Program for the Refinement of Crystal Structures. University of Göttingen, Germany, 1997.
32. Mackay, S.; Edwards, C.; Henderson, A.; etc. MaXus: a computer program for the solution and refinement of crystal structures from diffraction data. University of Glasgow, Scotland, 1997.
33. D. Waasmaier and A. Kirfel, *Acta Crystallographica* A., 1995, **51**, 416-430.
34. M. J. Frisch, et al. Gaussian 09, Revision D.01. Computer Program. 2013.
35. H. Iikura, H. Iikura, T. Tsuneda, T. Yanai, and K. Hirao, *the Journal of Chemical Physics*, 2001, **115**, 3540-3544.
36. M. Kamiya, H. Sekino, T. Tsuneda, and K. Hirao, *the Journal of chemical physics*, 2005, **122**, 234111.
37. W. Jin, P. V. Johnston, D. L. Elder, A. F. Tillack, B. C. Olbricht, J. Song, P. J. Reid, R. Xu, B. H. Robinson, and L. R. Dalton, *Appl. Phys. Lett.*, 2014, **104**, 243304.
38. S. Huang, T. Kim, J. Luo, S. K. Hau, Z. Shi, X. H. Zhou, H. L. Yip, and A. K. -Y. Jen, *Appl. Phys. Lett.*, 2010, **96**, 243311.